2007

Uranium(VI) Release from Contaminated Vadose Zone Sediments: Estimation of Potential Contributions from Dissolution and Desorption

Deborah L. Bond
U.S. Geological Survey, dlstoliker@usgs.gov

James A. Davis
U.S. Geological Survey

John M. Zachara
Pacific Northwest National Laboratory, john.zachara@pnl.gov

PNNL-SA-58541

Uranium(VI) Release from Contaminated Vadose Zone Sediments: Estimation of Potential Contributions from Dissolution and Desorption

Deborah L. Bond[*,†], James A. Davis[†], and John M. Zachara[‡]

[†] U.S. Geological Survey, Menlo Park, CA 94025

[‡]Pacific Northwest National Laboratory, Richland, WA 99352

Accepted for publication in *Adsorption of Metals to Geomedia II*

eds. M.O. Barnett and D.B. Kent

February 2007

*Corresponding author phone: 650-329-4529, fax: 650-329-4545, email: dlstoliker@usgs.gov

Published in Developments in Earth and Environmental Sciences, Volume 7, 2007, Pages 375–416
doi: 10.1016/S1571-9197(07)07014-0

Abstract – A key difficulty in developing accurate, science-based conceptual models for remediation of contaminated field sites is the proper accounting of multiple coupled geochemical and hydrologic processes. An example of such a difficulty is the separation of desorption and dissolution processes in releasing contaminants from sediments to groundwaters; very few studies are found in the literature that attempt to quantify contaminant release by these two processes. In this study, the results from several extraction techniques, isotopic exchange experiments, and published spectroscopic studies were combined to estimate the contributions of desorption and dissolution to U(VI) release from contaminated sediments collected from the vadose zone beneath former waste disposal ponds in the Hanford 300-Area (Washington state).

Vertical profiles of sediments were collected at four locations from secondary pond surfaces down to, and slightly below, the water table. In three of the four profiles, uranium concentration gradients were observed in the sediments, with the highest U concentrations at the top of the profile. One of the vertical profiles contained sediments with U concentrations up to 4.2×10^{-7} mol/g (100 ppm). U(VI) release to artificial groundwater solutions and extracts from these high-U concentrations sediments occurred primarily from dissolution of precipitated U(VI) minerals, including the mineral metatorbernite, $[Cu(UO_2PO_4)_2 \cdot 8H_2O]$. At the bottom of this profile, beneath the water table, and in all three of the other profiles, U concentrations were $<5.88 \times 10^{-8}$ mol/g (14 ppm), and U(VI) release to artificial groundwater solutions occurred primarily due to desorption of U(VI). When reacted in batch experiments with artificial groundwater solutions with compositions representative of the range of chemical conditions in the

underlying aquifer, all samples released U(VI) at concentrations greater than regulatory limits within a few hours.

A semi-mechanistic surface complexation model was developed to describe U(VI) adsorption on sediments collected from near the water table, as a function of pH, alkalinity, and Ca and U(VI) concentrations, using ranges in these variables relevant to groundwater conditions in the aquifer. Dilute (bi)carbonate solution extractions and uranium isotopic exchange methods were capable of estimating adsorbed U(VI) in samples where U(VI) release was predominantly due to U(VI) desorption; these techniques were not effective at estimating adsorbed U(VI) where U(VI) release was affected by dissolution of U(VI) minerals. The combination of extraction and isotopic exchange results, spectroscopic studies, and surface complexation modeling allow an adequate understanding for the development of a geochemical conceptual model for U(VI) release to the aquifer. The overall approach has generic value for evaluating the potential for release of metals and radionuclides from sediments that contain both precipitated and adsorbed contaminant speciation.

1. INTRODUCTION

Uranium (U) is a pollutant of concern in the United States due to subsurface contamination at numerous sites (Crowley and Ahearne, 2002). At many of these sites, groundwater plumes with high concentrations of U(VI) and other contaminants have developed (Riley et al., 1992), some of which discharge to rivers. For example, a groundwater plume with elevated concentrations of dissolved U(VI) underlies the North and South 300 Area Process Ponds in the 300-FF-5 Operable Unit at the Hanford site in Washington state (Fig. 1). The infiltration basins at this site operated from 1943 to 1975, receiving various waste streams containing high concentrations of U, Cu, F, Al, and nitrate, and the pH of the wastewater in the ponds varied temporally from 2-11 (Zachara et al., 2005).

Concentrations of U(VI) in the groundwater plume beneath the site have been persistently greater than expected (Zachara et al., 2005). Despite removal of highly contaminated pond bottom sediments (>4.2 μmol/g or 1000 ppm U), studies indicate that the 20-30 ft vadose zone beneath the infiltration ponds likely serves as a continuing source of U(VI) to the groundwater plume (Qafoku et al., 2005; Catalano et al., 2006). A geochemical model to evaluate the release of U(VI) from the sediments is needed as part of an overall conceptual model for the 300-Area site. The conceptual model will assist in understanding the expected longevity of the groundwater plume and its impact on the Columbia River, which is located ~300 feet to the east of the former infiltration ponds (Fig. 1). U(VI) is transported downward within the vadose zone as it is released from the contaminated sediments during the relatively wet season, and small amounts of drainage may reach the water table. The hydrologic model for the vadose zone is complex. At

high stages of the Columbia River, the groundwater table rises into the lower vadose zone (Lindberg and Peterson, 2004), leading to a condition in which the deeper vadose zone sediments may serve as both a source and sink for U(VI) in the system (Qafoku et al., 2005).

The geochemical conceptual model needs to be based on data from several different sources: 1) the conditions at the field site (groundwater compositions, redox status, etc.), 2) batch U(VI) water-sediment partitioning experiments, 3) long-term U(VI) release kinetic experiments, and 4) sediment characterization studies. Spectroscopic characterization of the vadose zone sediments has determined that U chemical speciation (Fig. 2) consists of: a) U(VI) co-precipitated with calcite in the pond bottom and the uppermost vadose zone sediments (Wang et al., 2005; Catalano et al., 2006), b) U(VI) precipitated as metatorbernite, $[Cu(UO_2PO_4)_2 \cdot 8H_2O]$ and other U(VI) minerals, at upper to intermediate depths in the vadose zone (Catalano et al., 2006; Arai et al., 2007), and c) U(VI) adsorbed onto phyllosilicates at deeper depths in the vadose zone and extending into the saturated zone (Catalano et al., 2006). Hence, there is an important need at this site (and many other metal-contaminated sites) to have the capability to estimate the separate contributions of desorption and dissolution as release mechanisms.

U(VI) desorption kinetics from the deeper vadose zone sediments are slow, contributing to significant retardation during transport and extensive tailing (Qafoku et al., 2005). Because of the presence of precipitated and co-precipitated U(VI) in the uppermost vadose zone sediments, the release of U(VI) to infiltrating precipitation can also be expected to be complex. In this chapter, we present the results of kinetic desorption and dissolution experiments conducted with depth sequences of vadose zone

sediments collected from four pits excavated beneath the 300-Area infiltration ponds. Various extraction and uranium isotopic exchange techniques were employed to estimate the fraction of total sediment U which is available for potential release to the groundwater plume during vadose zone recharge or temporal flooding. When combined with previous spectroscopic studies (Catalano et al., 2006; Arai et al., 2007), a conceptual geochemical model for the vadose zone sediments can be developed, with estimates of the potential contributions from dissolution and desorption to U(VI) release from the sediments in representative groundwater solutions. A semi-mechanistic surface complexation model is calibrated to describe U(VI) adsorption-desorption equilibria for the deeper vadose zone sediments as a function of pH, alkalinity, and Ca and U(VI) concentrations, similar to the approach used in other studies (Davis et al., 2002; 2004a). Variables were studied over ranges that are relevant to the groundwater in the aquifer beneath the site. The surface complexation model makes it possible to estimate separate contributions to U(VI) release from dissolution and desorption from the more highly contaminated sediments in the upper vadose zone.

2. MATERIALS AND METHODS

2.1. Site Description

Samples were collected from the 300-Area North and South Processing Ponds at the Hanford site, two main disposal basins that overlay different concentration regions of the U(VI) plume (Fig. 1). The ponds served as liquid disposal units from 1943-1975, receiving cooling water and low-level liquid wastes from fuel fabrication facilities including U, copper, cobalt and plutonium (Zachara et al., 2005). The pH of the waste varied widely due to the addition of acidic U(VI)/Cu(II) and basic sodium-aluminate

solutions. Sodium hydroxide was added to the former waste streams to impede migration of copper through the aquifer to the Columbia River. Between 30,000 and 60,000 kg of U were disposed in the ponds (USDOE, 2005). During the period between 1948 and 1975, several unplanned releases of holding effluent occurred (USEPA, 1996). The result of these leaks and additional seepage into the vadose zone are evident in the U(VI) plume emanating from the South Processing Pond (Fig. 1).

In 1996, following EPA recommendations (USEPA, 1996), 640,000 tons of contaminated soil were removed from the ponds to a waste disposal site. Additionally, in order to reduce the source of contamination from the ponds, several feet (ft) of sediment were scraped from the pond bottoms during 2001-2002, exposing a secondary surface. In 2003, two pits were excavated within each pond from the secondary surface down to the water table, approximately 20 ft below ground surface (bgs). The pits are referred to as NPP1, NPP2, SPP1, and SPP2; locations are shown in Figure 1. Sediments were collected by excavator from these pits at intervals of 2 or 4 ft. Sample designations identify the pit and depth below the secondary pit surface, e.g. North Processing Pit #1, 16 feet bgs is designated NPP1-16. The water table was located at approximately 22 feet bgs. The elevations of the samples relative to the water table are shown in Figure 3. One sediment sample from each pit was collected from beneath the water table.

Particle size in the samples ranged from clay-sized to cobbles, with river cobbles accounting for more than 65% of the mass. Samples identified as "groundwater fines" were collected separately as suspended material in groundwater that began to infiltrate the pits as excavation approached the water table. Generally, total U concentrations were at or below detection ($<2x10^{-8}$ mol/g) in the size fraction ranging from 2.0 to 75 mm

(Zachara et al., 2005). Sediments (19 samples from the 4 pits) were air-dried and sieved to <2 mm size fraction.

2.2. Surface Area Measurements

Specific surface areas were determined by N_2 adsorption at 77.35°K (Micromeritics Tristar 3000) under atmospheric pressure. Samples were heated to 40^{o}C and degassed under N_2 gas for ~20 hours. Measurements were made using the five-point method on 1 g sample masses. Surface areas of the groundwater fines were measured by Quantachrome Corporation (Boynton Beach, FL).

2.3. Total Uranium and Copper Content

Total U content was measured for each sample (< 2 mm) by non-destructive γ-spectrometry. ^{238}U was determined by measurement of the ^{234}Th daughter 63 KeV gamma ray emission line, assuming secular equilibrium in the sample (Davis and Curtis, 2003). ^{235}U was determined from its 186 KeV gamma ray after correction for the ^{226}Ra contribution to this energy region. The ^{226}Ra correction was based on measurement of its gamma-emitting daughters. Copper (Cu) content of sample material was obtained by energy dispersive x-ray fluorescence spectroscopy (KEVEX 0810A system) at Pacific Northwest National Laboratory (PNNL) utilizing the backscatter fundamental parameter approach. Solid samples were pelletized from approximately 500 mg of dry material (<149 micron) into a 3 cm wafer. The x-rays were detected by a cryogenically cooled solid state lithium drifted silicon (Si(Li)) detector connected to a multi-channel analyzer. The method of peak analysis is described in Nielson (1978).

2.4. Hydroxylamine-Hydrochloride (HH) Extractions and Ammonium Oxalate Extractions

Hydroxylamine-hydrochloride extractions were performed in duplicate to dissolve and estimate the abundance of poorly crystalline iron hydroxides (Chao and Zhou, 1983) in selected sediment samples. Two hundred g of 0.25 M $NH_2OH{\cdot}HCl$ in 0.25 M HCl at 50°C were added to 10 g of sediment in a 250 mL bottle and placed in a water bath at 50°C. The bottles were shaken mechanically and sampled at 30 minutes.

Ammonium oxalate (AMOX) extractions were performed as a second method to dissolve and estimate the abundance of poorly crystalline iron (oxy)hydroxides (Chao and Zhou, 1983). Two hundred mL of 0.12 M oxalic acid and 0.11 M ammonium oxalate (pH ~3) were added to 5 g of sediment in foil-wrapped 250-mL centrifuge bottles and shaken mechanically for 4 hours at room temperature in the dark.

For both extractions, an aliquot of the extract was transferred to a polycarbonate centrifuge tube and centrifuged to remove solids. From the supernatant, a sub-sample was converted to its nitrate salt by ad-mixing concentrated nitric acid and hydrogen peroxide followed by evaporation to dryness (Davis and Curtis, 2003). The solid was reconstituted in 0.15 M HNO_3 and analyzed for U(VI) by kinetic phosphorescence analysis (KPA). The remainder of the supernatant was filtered through a 0.45 μm PVDF filter and diluted with 0.15 M HNO_3 for analysis by inductively coupled plasma – atomic emission spectroscopy (ICP-AES).

2.5. Dithionite Citrate Bicarbonate Extractions

Dithionite citrate bicarbonate (DCB) extractions were performed in duplicate to estimate the abundance of crystalline iron oxides in selected sediment samples (Chao and Zhou, 1983). Two hundred mL of 0.30 M sodium citrate, 0.20 M sodium bicarbonate, and 0.14 M sodium dithionite (pH ~8.3) were added to 5 g of sediment in a 250 mL

centrifuge bottle and placed in a water bath at 85°C. The bottles were shaken mechanically and sampled after 0.5 hr. The bottles were centrifuged, supernatant collected, and the extraction was repeated. The samples were centrifuged again and the leachates were combined. Samples were processed and analyzed by KPA and ICP-AES in the manner described above. The authors recognize that U(VI) released in these extractions is not necessarily associated with the dissolving crystalline iron oxide phases. However, useful comparative information can be obtained by putting the results of the extraction in context with the results from other extraction methods.

2.6. Formate Buffer Extractions

Formate buffer extractions were conducted to estimate the quantity of U(VI) that was either sorbed U(VI) or present in mineral phases that could be dissolved by dilute acid, e.g. U(VI) co-precipitated within carbonates or poorly crystalline oxides. Sodium formate (0.5 M) was acidified to pH 3.5 with formic acid and added to sediments at a suspension density of 50 g/L in 500 mL. We are unaware of a previous publication discussing the use of formate buffer as an extractant. It was chosen as an extractant here because of its ability to: 1) dissolve poorly crystalline hydrous iron oxide and aluminum oxide phases (but not crystalline hydrous iron oxide phases) at pH 3.5 (Chao and Zhou, 1983), 2) expected complete desorption of U(VI) from oxide surfaces (Payne et al., 1998), and 3) dissolve carbonate mineral phases. The technique should be more quantitative at releasing U(VI) co-precipitated with carbonate mineral phases than acetate buffer extractions (pH 4.7), because any released U(VI) will likely not be re-adsorbed at pH 3.5 (Payne et al., 1998). Bottles were placed on an orbital shaker at room temperature and subsampled at various times up to 4 weeks. The pH varied minimally during the

extractions, typically by only 0.05 pH units. Samples were processed and analyzed by KPA and ICP-AES in the manner described above.

In a few samples (NPP2-2, NPP2-4, and NPP 2-8), extracted copper concentrations were in excess of 1 mM. For these samples, the KPA method was less effective for measurement of U(VI) due to quenching effects. Dissolved U(VI) concentrations for these samples were measured instead by ICP-AES, as the concentrations were well within the detection limit for this instrument.

2.7. Dilute (Bi)carbonate Extractions

Dilute (bi)carbonate extractions were conducted to determine the amount of U(VI) released from the sediment samples under moderately alkaline conditions. A solution consisting of 1.44×10^{-2} M $NaHCO_3$ and 2.8×10^{-3} M Na_2CO_3 at pH 9.45 was added to the sediments in a ratio of 50 g/L, following the approach of Kohler et al. (2004). The ionic strength and alkalinity of the solution are 0.022 M and 20 meq/L, respectively. The bottles were placed on an orbital shaker at room temperature and sampled at various times for at least 3 weeks. The extractions were performed in duplicate and pH values were measured at each time point. Samples were removed by allowing the suspension to settle and removing an aliquot of supernatant for centrifugation. For KPA analysis, a sub-sample of centrifugate supernatant was diluted with 0.15 M HNO_3 for analysis. ICP-AES samples were filtered (0.45 μm) and diluted in 0.15 M HNO_3 prior to analysis.

For most samples, the pH of the extract initially dropped <0.5 pH units and remained higher than 8.8 throughout the extraction. However, during extractions of the groundwater fines samples, the pH dropped to 8.5 within the first hour of extraction and

remained constant thereafter. As reported in Kohler et al. (2004), it is important to keep the pH above 8.8 during the extraction to avoid reaching conditions at which released U(VI) would begin to readsorb. Extractions of the groundwater fines samples were repeated at lower suspension densities (20 g/L) to maintain a pH≥8.8 and prevent U(VI) adsorption. Possible re-adsorption of extracted U(VI) was evaluated at the end of (bi)carbonate extractions by addition of ^{233}U(VI) isotope and measurement of tracer activity for 24 hrs. No re-adsorption was measured for samples with pH above 8.6 (within 5% error).

2.8. Artificial Groundwater Experiments

Sediments were reacted with artificial groundwater solutions (AGWs) with varying alkalinity and ionic strength to determine the amount of U(VI) released as a function of chemical conditions. The initial composition of the artificial groundwaters (Table 1) was based on the range of well water compositions in the 300-Area (Serne et al., 2003). The initial pH (Table 1) refers to the pH of each AGW prior to contact with the sediments. To study U(VI) desorption as a function of alkalinity, a series of groundwaters (AGW2-6, 12-13) was prepared with varying bicarbonate concentration. The concentrations of other major solutes were kept nearly constant and varied only to obtain waters with similar ionic strength. The composition of AGW2 was close to saturation with respect to calcite, while the other AGW solutions were significantly undersaturated (prior to sediment addition). Another series of groundwaters (AGW8-11) were synthesized to mimic AGW3-6, except with ionic strength increased to I = 0.1 M by addition of sodium nitrate. Groundwaters were filtered (0.45 μm) prior to contact with sediments.

The batch experiments were conducted with variable suspension densities (25 – 1600 g/L) of sediment in polyethylene centrifuge tubes or bottles placed on a shaker table for up to 2 weeks. Some centrifuge tubes were also mixed on an end-over-end rotator (14 rpm) for method comparison and showed no statistical difference in results. Individual tubes were sacrifice-sampled during the course of the experiments, and the pH was measured immediately. The alkalinity of each sample was measured on a filtered, unacidified aliquot. Samples were then centrifuged (16,270 g RCF for 10 min) and an aliquot of supernatant was diluted with 0.15 M HNO_3 for KPA analysis. Centrifugation was preferred as a method of phase separation to avoid U(VI) sorption onto filters. Sorption of U(VI) to sample-tubes was monitored with control samples of U(VI) spiked AGW and solution concentration remained constant over time. ICP-AES samples were filtered (0.45 μm) prior to dilution with 0.15 M HNO_3 and analysis.

The pH in all AGW experiments was well buffered by the carbonate alkalinity of the water and the buffer capacity of the sediments. There was some variability in pH, depending on the initial alkalinity, ionic strength, and solid:liquid ratio in each experiment. The range of pH observed among the combinations of low ionic strength groundwater solutions and sediment samples for pits NPP1, SPP1 and SPP2 was 7.9 ± 0.3. Sediment samples from the NPP2 pit yielded a lower pH range of 7.1 ± 0.3. Experiments conducted with AGWs 8-11 (higher ionic strength) had slightly higher pH values. For example, sediments reacted with AGW9 equilibrated at pH 8.3 ± 0.1.

2.9. U(VI) Isotopic Exchange Experiments

Isotope exchange experiments were conducted following a modified approach of Kohler et al. (2004) to determine "labile" abundances of sediment U(VI). Variable

suspension densities (25 to 200 g/L) were used to control the concentration of U(VI) in solution, in order to accurately measure ^{233}U(VI) activity. Prior to the addition of the ^{233}U(VI) isotope, the sediments were reacted with AGW4 (see section 2.8) for either: 1) 24 hr, or 2) 1260 hr. The latter reaction time allowed the achievement of near steady-state dissolved U(VI) concentrations (<2% change per week) prior to the isotope addition. Subsamples were collected for pH, alkalinity, U(VI) concentration, and background activity (measured by LSC, liquid scintillation counting) prior to isotope addition, and then the suspensions were spiked with a ^{233}U secondary stock to achieve a concentration of 4-10x10^{-9} M ^{233}U(VI) (20-50 dpm/mL). The sediments were then shaken for up to 3400 hr, with aliquots removed periodically and measured for pH, alkalinity, ^{233}U activity by LCS, and U(VI) concentration by KPA. Exchangeable ("labile") U(VI) in the sediment was then determined by:

$$C_{Labile} = \frac{A_{System}}{A} \cdot C \qquad (1)$$

where C_{Labile} is the concentration (moles/L) of the exchangeable U(VI), A_{System} is the total ^{233}U activity (dpm/L) in the system, A is the activity of dissolved ^{233}U (dpm/L), and C (moles/L) is the concentration of dissolved U(VI) (Kohler et al., 2004). Corrections were made for 1) ^{233}U and U(VI) removed during sampling and 2) the contribution of ^{233}U to total system uranium concentration. Addition of the ^{233}U(VI) spike increased the dissolved U(VI) concentrations in the experiments by 0.2 to 5.4% (average = 1.0%).

2.10. U(VI) Sorption Isotherms

In order to develop a U(VI) sorption isotherm, experiments were conducted for selected deeper pit samples suspended in AGW4 with added U(VI). Solutions were prepared by adding U(VI) (100 mg/L in 2% HNO_3) to AGW4 or AGW9, followed by a

small adjustment of the pH to the original pH value. These solutions were stored overnight to allow equilibration of aqueous U(VI) speciation at the higher U(VI) concentration.

Sediment samples in the experiments were pre-treated by suspension in AGW4 or AGW9 for 72 hr, after which the pH was measured and the tubes were centrifuged. Supernatant was collected to measure alkalinity, U(VI) concentration (by KPA), and water composition determined by ICP-AES. Following the pre-treatment, weighed aliquots of U(VI)-spiked groundwater were added to each centrifuge tube. Tubes were sacrificed-sampled up to 100 hr of reaction time. Alkalinities remained stable and pH in the experiments was relatively constant with time for each sediment sample, but varied from 7.9 to 8.25 among the sediment samples and at different solid:liquid ratios. Samples were centrifuged and processed for analysis by ICP-AES and KPA.

2.11. Modeling

FITEQL 4.0 (Herbelin and Westall, 1999) was used for aqueous speciation and surface complexation modeling. The Davies equation was used for activity correction of aqueous species only. Thermodynamic data (Table 2) used in the modeling are consistent with the most recent NEA database for uranium (Guillaumont et al., 2003), except the aqueous ternary species, $CaUO_2(CO_3)_3^{2-}$ and $Ca_2UO_2(CO_3)_3^0(aq)$ (Kalmykov and Choppin, 2000; Bernhard et al., 2001), were also included. Calcite equilibrium in the experiments was not assumed; measured dissolved Ca values were used as FITEQL input and neither calcite precipitation nor dissolution was included in the calculations. FITEQL 4.0 was used to determine the best fit of various U(VI) surface reactions or combinations of reactions to experimental data in model calculations using a semi-mechanistic

modeling approach (Davis et al., 2004a). Relative errors of 1% in the concentrations of surface sites, 3% in total U(VI), 4% in adsorbed U(VI), and 5% in log [H^+] and log [H_2CO_3] were used as FITEQL input values. The purpose of the surface complexation model developed here is twofold: 1) to estimate U(VI) adsorption in samples from the sediment profile that may contain both adsorbed and precipitated U(VI), and 2) to provide a quantitative estimate of U(VI) adsorption-desorption equilibria for future reactive transport simulations of U fate and transport in the vadose and saturated zones of the aquifer underlying the former disposal ponds. As in previous work with this non-electrostatic modeling approach (Davis et al., 2004a; 1998), surface protonation and deprotonation reactions are not used.

3. RESULTS

3.1. Sediment Characterization

Mineralogical and particle size analysis of the bulk sediment and clay-sized fraction have been carried out in previous work (Serne et al., 2003; Catalano et al., 2006; Qafoku et al., 2005, Zachara et al., 2005). Diffraction analyses (Serne et al., 2003; Zachara et al., 2005) reveal nearly identical mineralogical assemblages in each of the 19 samples studied. Bulk XRD data of the <2 mm fraction indicate that sediments in the NPP-1 and SPP-2 pits are primarily composed of quartz, plagioclase feldspar, muscovite, and hornblende. The vadose zone sediments contain little or no calcite (<0.01% inorganic carbon), whereas the pond sediments and sample NPP2-0.5 (not studied in this paper) contained abundant calcite (Catalano et al., 2006; Qafoku et al., 2005). Extracted iron varied from 77-300 μmoles/g in the deeper pit samples and fines (Table 3), presumably present primarily as hydrous iron oxides, with 30-60% of the iron oxides present as

poorly crystalline iron (HH and AMOX compared with Fe in DCB extractions). Iron dissolved by the HH and AMOX methods varied significantly by method, suggesting that iron oxide phases of intermediate crystallinity were present. Microscopic studies of thin sections of the deeper vadose zone sediments (near the water table) showed that larger sediment grains were coated with thin layers of phyllosilicates (e.g., smectite, vermiculite, and chlorite) that were identified by X-ray diffraction of the clay-sized fraction (J.P. McKinley, personal communication). The poorly crystalline iron hydroxide phases likely result from the weathering of chlorite in the grain coatings. Surface area ranged from 15 to 27 m^2/g among the pit samples; groundwater fines ranged from 41 to 54 m^2/g (Table 4).

Values of total U concentration in the <2 mm sediment samples ranged from $1.2x10^{-8}$ to $6.6x10^{-7}$ mol/g (2.9 to 157 ppm) (Table 4). The average mass ratio of ^{235}U to ^{238}U for all samples was 0.0084 ± 0.0011 in agreement with the natural mass abundance ratio of 0.0073. Total U values measured by γ-spectrometry agree reasonably well with measurements made by x-ray fluorescence spectroscopy (J.M. Zachara, personal communication). NPP2 pit samples contained the highest U concentrations, nearly 10 times that of the other pit samples. In contrast to the other pits, the high U concentrations extended down to the water table (Fig. 3). With the exception of pit SPP1, total U concentrations decreased with depth. Excluding pit NPP2, total U concentrations ranged from $1.2x10^{-8}$ to $4.0x10^{-8}$ mol/g (2.9 to 9.6 ppm) in sediments near the water table, compared to background values near $5.0x10^{-9}$ mol/g (1.2 ppm) for Hanford sediments (Serne et al., 2003). The fines samples, collected from the water table, contained total U concentrations ranging from $5.5x10^{-8}$ to $6.6x10^{-7}$ mol/g (13 to 157 ppm), with the NPP2-

fines samples considerably greater than the other three pits. The groundwater fines were collected as suspended material in groundwater that infiltrated the pits during sampling of sediments beneath the water table.

Dissolved U(VI) concentrations were determined in the extractions of selected deep pit samples that were conducted to dissolve iron oxide phases (Table 3). Eighty percent or more of the total U was dissolved or desorbed from NPP1 sediments in the HH and AMOX extractions, and essentially 100% in DCB extractions. SPP2 deep pit samples released a lower percentage of total U, ranging from 50-75% in the HH and AMOX extractions, and 70-100% during the DCB extractions. Between 92% and 96% of total U was dissolved from the groundwater fines samples during these extractions. The results do not mean that U(VI) released in these extractions was necessarily associated with the phases dissolved. For example, the low pH of the HH extraction can likely cause U(VI) desorption from any mineral phase in the sample.

3.2. Formate Buffer Extractions

Formate extractions (pH 3.5) were conducted to measure elemental release as a function of time under dilute acidic conditions. U(VI) concentrations increased rapidly at the beginning of the extraction and appeared to reach steady-state at 24 hr. Formate-extractable U ranged from 7.3×10^{-9} to 3.4×10^{-7} mol/g (Table 4), equivalent to 61-107% of the total U in the samples (Table 5). In addition to U, high concentrations of copper (Cu) were dissolved from samples NPP2-2 and 2-4 (Table 4), and the extractions removed more than 92% of total Cu in these samples. Catalano et al. (2006) suggested that around 50% of U in sample NPP2-4 was present as metatorbernite, and the high percentages of

total U and Cu dissolved in this sample suggest that the formate extraction was efficient in dissolving metatorbernite.

The pH and ionic strength conditions of the extraction should achieve essentially complete desorption of U(VI) from most mineral surfaces, either as surface complexes or from ion exchange sites in aluminosilicate minerals (Payne et al., 1998; Turner et al., 1996). In addition, poorly crystalline iron oxide/aluminosilicate phases and trace calcite may be dissolved under these conditions, releasing any co-precipitated U(VI). For sample SPP2-18, 39% of the total U was not extracted; this is equivalent to 4.6×10^{-9} mol/g U (1.1 ppm), which is near the concentration of background U in Hanford sediments (Serne et al., 2003). Most of the background U is sequestered within the crystal matrices of silicate minerals, rather than present on mineral surfaces, and thus would not be expected to dissolve in chemical extractions other than hydrofluoric acid.

3.3. Dilute (Bi)carbonate Extractions

Kohler et al. (2004) found that a dilute (bi)carbonate extraction method could be used to estimate adsorbed U(VI) on aquifer sediments that were contaminated in the range of 1.3×10^{-8} - 3.4×10^{-8} mol/g total U (3-8 ppm). The basis of the method is to desorb U(VI) by strong aqueous complexation with carbonate at pH 9.0-9.5, allowing for minimal dissolution of crystalline mineral matrices in comparison with harsher extraction methods. U(VI) speciation calculations with FITEQL (Herbelin and Westall, 1999) suggest that more than 98% of dissolved U(VI) is present as $UO_2(CO_3)_3^{4-}$ under the extraction conditions.

Figure 4 shows the pH and concentrations of dissolved calcium and U(VI) in the dilute (bi)carbonate extraction of the deep vadose zone sample, NPP1-16, as a function of

time. Calcium (Ca) concentrations dropped rapidly during the first 4 hr of the extraction, and then stabilized, likely as a result of a small amount of calcite precipitation at the beginning of the extraction. Separate experiments have shown that calcite is not dissolved by the dilute (bi)carbonate extraction (D. Bond, unpublished results). U(VI) desorbs rapidly during the first 72 hr of the extraction, but U(VI) concentrations continued to increase slowly for weeks thereafter (Fig. 4). The range of U(VI) released by the (bi)carbonate extraction was 19 to 58% of total U (Table 5).

3.4. Artificial Groundwater Extractions

3.4.1. Aqueous compositions

U(VI) dissolution and desorption from the sediment samples was studied in artificial groundwaters of varying composition (Table 1) in order to determine the effects of ionic strength, pH, alkalinity, Ca concentration, U(VI) concentration, and solid:water ratio on the rate and extent of U(VI) release to the aqueous phase. It was not possible to independently control these variables in the experiments, as the sediments exerted a strong influence on the aqueous composition, specifically the pH and Ca concentrations. Figure 5 shows the evolution in concentration of some major elements in the water during a typical extraction of a deep vadose zone sample (e.g., NPP1-16) with AGW4. Calcium, magnesium (Mg), and silicon are released from the sediments rapidly at first, and then continue to increase slowly in concentration for a few weeks. Sodium solution concentrations decrease with time due to ion exchange.

One of the main differences in the initial compositions of the artificial groundwaters was dissolved bicarbonate (Table 1). The measured alkalinities of several artificial groundwaters during the reaction of sample NPP1-20 is shown as a function of

time in Figure 6. With the exception of AGWs 12 and 13, alkalinity generally remained constant during the experiments. For AGWs 12 and 13, alkalinity decreased rapidly during the first few hours of the experiments and then stabilized, suggesting that calcite precipitation may have occurred in the beginning of the experiments with AGWs 12 and 13, but not in the other AGW experiments. With the exception of AGWs 5 and 6, the waters were calculated to be oversaturated with respect to calcite for the duration of the experiments, and the degree of calcite saturation was well correlated with the alkalinity of the solution (Fig. 7). Partial pressures of carbon dioxide gas in the headspace of the experimental tubes after 96 hr of reaction were calculated from the measured pH values and alkalinities (assuming carbonate species only contributed to alkalinity). The pH values and partial pressures of carbon dioxide gas ranged from 7.6 to 8.4 and 0.05-0.6% in the experiments, respectively, in AGW batch experiments with sediment samples collected near or beneath the water table. This range of values is representative of existing conditions in Hanford groundwaters beneath the 300-Area, including conditions expected from the mixing of regional groundwater with river water.

Inhibition of calcite nucleation or crystal growth likely caused the observed oversaturation with respect to calcite in the batch experiments. Inhibition has been observed when solutions contain anions, such as phosphate or dissolved organic carbon (DOC) (Reddy and Wang, 1973; Inskeep and Bloom, 1986; Dove and Hochella, 1993; Lebron and Suarez, 1996). Calcite precipitation was greatly inhibited in the range of 0.02-0.15 mM DOC (as C) with a saturation index (SI) equal to 0.95 (SI = log [IAP/Ksp]) (Lebron and Suarez, 1996). In AGW4 experiments with samples NPP1-16 and SPP2-18, DOC values were measured at 0.13 and 0.025 mM (as C), respectively, with SI $\approx$ 0.4.

Similar DOC values were measured in AGWs 5 and 13 for both sediment samples (SI ≈ -0.2 and 0.8). Calcite seeding after 72 hr of reaction had minimal effects on the degree of oversaturation in the batch experiments, consistent with the hypothesis that inhibition of calcite nucleation or crystal growth caused the observed oversaturation.

The speciation of dissolved U(VI) in the AGW is complex, and unfortunately, subject to some thermodynamic uncertainty. FITEQL was used to calculate the expected speciation of a 2 μM U(VI) solution in a closed system at pH 7.87 as a function of alkalinity (assuming only carbonate species contribute to alkalinity), with the aqueous phase assumed to be at equilibrium with calcite (Fig. 8). The predicted predominant species for these solutions is $Ca_2UO_2(CO_3)_3$ (aq), except at the highest alkalinity values, where the $UO_2(CO_3)_3^{4-}$ species becomes important. The $Ca_2UO_2(CO_3)_3$ (aq) species is known to exist in Hanford groundwaters (Wang et al., 2004; Dong et al., 2005), but precise calculation of its concentration with thermodynamic calculations is subject to some uncertainty at present (Guillaumont et al., 2003). Despite the uncertainty, it is important to include the $Ca_2UO_2(CO_3)_3$ (aq) species in calculations, because its formation has been shown to decrease U(VI) adsorption (Fox et al., 2006; Dong et al., 2005). The calculations shown in Figure 8 and elsewhere in this paper assume a log K value of 30.0 for the $Ca_2UO_2(CO_3)_3$ (aq) species, consistent with the calculations in Fox et al. (2006).

3.4.2. U(VI) release to solution

Aqueous concentrations of U(VI) increased rapidly during the first 24 hr of reaction between artificial groundwaters and Hanford sediments, as illustrated in Figure 9 for the deep vadose zone samples. After 24 hr, a steady slow release of U(VI) continued. The slow release of U(VI) did not appear complete after 7 weeks of reaction, at which

point the experiments were ceased. Figures 10 and 11 show that as the alkalinity of the artificial groundwaters increased, the release of U(VI) increased. The impact of ionic strength on U(VI) desorption was minimal, and desorption experiments with greater suspension density had lower concentrations of desorbed U(VI) per unit mass of sediment (Fig. 12). The dependence of desorption on suspension density is a consequence of the mass law for adsorption-desorption equilibrium; as the suspension density increases at constant aqueous conditions, the surface site concentration increases, which favors adsorption over desorption.

As noted above, many of these experiments were carried out in solutions that were supersaturated with respect to calcite. Previous studies of uranyl co-precipitation within calcite report partitioning coefficients near 0.1 (Meece and Benninger, 1993; Reeder et al., 2001). Assuming that all of the initial bicarbonate ion lost from solution in AGWs 12 and 13 (Fig. 6) was precipitated as calcite, and that U(VI) was co-precipitated with calcite with a partitioning coefficient of 0.1, less than 1% of dissolved U(VI) would have been removed in the experiments by co-precipitation. Thus, the impact of any calcite precipitation on the evolution of dissolved U(VI) during the AGW experiments is expected to be within the experimental error of the measurements (0.2 to 8.6 %, see Table 5).

3.5. U(VI) Isotopic Exchange Experiments

U(VI) isotopic exchange was used to assess the "labile" fraction of U(VI) distributed between the aqueous and sediment phases, after reaction with AGW4 for either 24 hr or 1260 hr. In the case where sediment samples were reacted for 1260 hr, a relatively stable dissolved U(VI) concentration was obtained prior to addition of a

^{233}U(VI) spike to the aqueous phase. In the case of 24 hr for the initial reaction period, both total dissolved U(VI) and ^{233}U(VI) activity changed significantly as a function of time during isotopic exchange.

Figure 13a shows the concentration of dissolved U(VI) and the activity of the ^{233}U(VI) tracer in the isotopic exchange experiment conducted with the deep vadose zone sample, NPP1-16, after 24 hr of pre-equilibration with AGW4. The ^{233}U(VI) tracer activity in solution declined rapidly during the first 48 hr, and then began to decline at a slower rate that appeared to continue after 1350 hr of exchange. Dissolved U(VI) increased rapidly during the first 200 hr, and then reached a stable concentration near 0.8 μM after that. Figure 13b shows the variables for the same sample, but in this case, the sample was first pre-equilibrated with AGW4 for 1260 hr. The decline in ^{233}U(VI) tracer activity exhibited similar kinetic behavior, but in this experiment, dissolved U(VI) had already reached the stable concentration near 0.8 μM before the isotopic exchange was initiated.

Based on the fractional partitioning of ^{233}U(VI) tracer between the solid and liquid phases, the dissolved and total U(VI) concentrations, and the solid:liquid ratio, one can calculate a "labile" fraction of U(VI) associated with the sediment (see Eq. 1) (Kohler et al., 2004). The term "labile" fraction can only be operationally defined because of the evolving ^{233}U(VI) tracer activity with time; calculated values as a function of time are shown in Figures 13a and 13b. Labile U(VI) represents the mass of U(VI) that achieves isotopic equilibrium with the aqueous phase within the calculated time frame. ^{233}U(VI) likely exchanges first with adsorbed U(VI) on mineral surfaces exposed to bulk solution, because of the fast chemical reaction and the lack of a diffusion barrier in the well-mixed

bulk solution. Slower isotopic exchange then occurs with: 1) adsorbed U(VI) in micropores, due to mass transfer limitations, and 2) U(VI) present in precipitated or co-precipitated mineral phases, depending on kinetic constraints.

Note that calculated labile U(VI) reached nearly the same value for sample NPP1-16 regardless of the time allowed for pre-equilibration in AGW4 (compare Figs. 13a and 13b). This near equality of the final labile U(VI) values can be expected in the case where the predominant form of labile U(VI) in the sediment is adsorbed U(VI). The kinetic behavior can be contrasted with the case in which U(VI) dissolution is also occurring on the same time scale as U(VI) desorption. For example, Figure 14 shows similar data for sample NPP2-4, which contains a significant amount of precipitated U(VI). Because dissolution continues throughout the isotopic exchange experiment, the dissolved U(VI) concentration is much higher in the case of 1260 hr of pre-equilibration in AGW4 (at the time that ^{233}U tracer was added) and continued to rise even after isotopic exchange was initiated. As a result, calculated labile U(VI) was much higher at any point in the isotopic exchange experiments with sample NPP2-4 if 1260 hr of pre-equilibration was allowed rather than 24 hr (compare Figs. 14a and 14b). For sample NPP2-4, as precipitated U(VI), e.g. metatorbernite, dissolves during the pre-equilibration period, the mass of exchangeable U(VI) in the sample increases. Using an estimated solubility product of log K = -45 for the mineral, torbernite, aqueous speciation calculations suggest that the solution was about ten orders of magnitude undersaturated with respect to torbernite during these experiments, even after long periods of equilibration.

As will be discussed further below, we have assumed that the *labile mass* of U(VI) in the deeper pit samples (near the water table, e.g. NPP1-16, NPP1-20, SPP2-16,

SPP2-18) is composed solely of adsorbed U(VI), with the definition of labile U(VI) based on 336 hr of isotopic exchange (with 1260 hr of pre-equilibration in AGW4). Given that assumption, then the fractional amounts of U(VI) desorbed by various groundwater solutions can be calculated. Figure 10 illustrates that 44% of adsorbed U(VI) was desorbed in 96 hr from sample NPP1-16 (200 g/L) by AGW2 (alkalinity = 8 meq/L), whereas only 3% was mobilized by AGW5 (alkalinity = 1 meq/L). As mentioned above, the fraction desorbed was also dependent on the sediment:water ratio; AGW2 desorbed 82% or 52% of adsorbed U(VI) from suspensions of sample SPP2-18 (25 or 200 g/L, respectively). Qafoku et al. (2005) found that 69% of labile U(VI) was released to an artificial groundwater solution (similar to AGW2) during slow passage of 100 pore volumes through a column packed with sample SPP2-18. The authors found a similar value for labile U(VI) for sample SPP2-18 (2.68 nmoles/g) as that reported here (2.53±0.3 nmoles/g).

3.6. U(VI) Sorption Isotherm

U(VI) quickly sorbed to the sediment surfaces in these experiments (artificial groundwater spiked with $2x10^{-6}$ - $5x10^{-6}$ M U(VI), reaching a steady-state dissolved U(VI) concentration within 24 hr. Suspension density and concentration of U(VI) added were varied and combined with AGW4 desorption data (batch experiments without added U(VI)) to produce U(VI) isotherms for the deeper pit samples (near the water table, e.g. NPP1-16, NPP1-20, SPP2-16, SPP2-18) (Fig. 15). Ionic strength had a negligible effect on the amount of U(VI) adsorbed (AGW 4 vs. AGW 9). For the deep pit samples it was observed that NPP samples adsorbed U(VI) more strongly than the SPP samples (Fig. 15). The bulk mineralogy of these samples, however, is nearly identical, as are the

surface areas (average NPP = 20.4 m^2/g and SPP = 19.1 m^2/g). The samples vary in particle size distribution, with a higher percentage of clay/silt in the NPP samples, and the greater abundance of fine-grain material may explain the observed difference in U(VI) adsorption.

3.7. Surface Complexation Model

Based on the assumption that the *labile mass* of U(VI) in the deeper pit samples (NPP1-16, NPP1-20, SPP2-16, SPP2-18) is composed solely of adsorbed U(VI), a non-electrostatic surface complexation model for U(VI) adsorption on the sediments was developed using the generalized composite modeling approach (Davis et al., 2004a). The model provides a quantitative description of U(VI) sorption equilibria as a function of aqueous chemical conditions. All of the experimental data for the deeper pit samples was included in the model calibration. A total site density of 3.84 μmoles/m^2 was used in the model (Davis and Kent, 1990). Based on previous work (Davis et al., 2004a), nine monomeric U(VI) surface reactions (Table 6) were considered to describe U(VI) sorption by the sediments.

FITEQL calculations were first completed to determine which single surface reaction (Table 6) would provide the best fit to the experimental data. FITEQL output includes a goodness-of-fit parameter, WSOS/DF, the weighted sum of squares of the difference in value between model simulations and experimental data points, divided by the degrees of freedom (Herbelin and Westall, 1999). Lower values of WSOS/DF mean the proposed model is a better fit to the data; WSOS/DF is referred to as a "fit value" below.

Representing the U(VI) adsorption data with a single reaction produced a reasonable fit (fit values = 8.2 to 10.2), with the best fit values provided by reactions 1, 2, 3, or 4 (Table 6). The second step in model development was to consider combinations of two reactions to represent the data. In many cases, the fit to the data was improved by adding a second reaction, with the best combinations being reactions 2 and 3 (fit value = 7.3) or 2 and 6 (fit value = 7.7). Adding a second surface site (strong versus weak) only improved the fit marginally, perhaps because the log-log isotherm data (Figure 15) exhibit a slope near one, indicating a nearly linear isotherm. Very little improvement to the fit could be achieved by adding a third surface reaction; the best combination of three reactions was 2, 3, and 6, which only improved the fit from 7.29 to 7.27. This was not considered sufficient improvement to add reaction 6 to the model, and thus the recommended model to describe U(VI) adsorption in the 300-Area subsurface is a one-site model with reactions 2 and 3. Model parameters are given in Table 7.

The surface complexation model describes the U(VI) sorption data reasonably well (Figures 15 and 16) over the range of conditions considered in the experiments. However, the goodness-of-fit is clearly impacted by a difference in U(VI) adsorption between the NPP and SPP samples; a model calibrated with all data splits the two sets of experimental data. Models calibrated with data only from the NPP or SPP sediments are also shown in Figures 15 and 16 in order to estimate the effect of the sediment heterogeneity on model parameter values (Table 7).

Once the models were calibrated, the separate NPP and SPP models were used to *estimate* the amount of adsorbed U(VI) that was present on each sample, based on the amount of U(VI) released in the first few hours of equilibration with AGW4. The

individual models (NPP or SPP), not the composite, were used for estimating adsorbed U(VI) on samples from the two ponds. An assumption of the estimation method is that only U(VI) desorption was significant during the first few hours of equilibration. Obviously, samples that contain both adsorbed U(VI) and precipitated U(VI) can release U(VI) either by dissolution or desorption, so the estimation method is, at best, an overestimate of desorbed U(VI). Using kinetic U(VI) desorption data for samples NPP1-16 (Fig. 10) and SPP2-18, it was estimated from the shapes of the curves that steady-state dissolved U(VI) concentrations in AGW4 were approximately 1.5 times greater at equilibrium (after 96 hr reaction) than after 4 hr of U(VI) desorption from these samples. Using this ratio, dissolved U(VI) concentrations due to desorption alone in AGW4 were estimated for each sample based on the amount of U(VI) released after 4 hr. The surface complexation model was used to calculate the amount of adsorbed U(VI) that would be in equilibrium with the dissolved U(VI) concentrations (specific for each sample), given the aqueous chemical conditions in the experiment (pH, dissolved carbonate, Ca concentration, etc.). This allowed a calculation of adsorbed U(VI) for each sample prior to the reaction with AGW4; these quantities are given as a percentage of the total U for each sample in Table 5.

4. DISCUSSION

Catalano et al. (2006) used spectroscopic techniques to show that contaminant uranium in the depth sequence of vadose zone sediments is characterized by at least three types of uranium speciation: 1) U(VI) co-precipitated with carbonate minerals in the uppermost samples, close to the previous pond bottom, 2) U(VI) precipitated as metatorbernite and other phases (Arai et al., 2007) in samples about one meter below the

top of the sequence, and 3) sorbed U(VI) in the intermediate and deeper depths of the sediment profile, near the water table. Wang et al. (2005) argued that a portion of the U(VI) in the pond bottom sediments was associated with carbonate mineral surfaces, both as a sorbed surface species and co-precipitated within the mineral structure. The combination of extraction and isotopic exchange results across the vertical profile of vadose sediments presented here allows a qualitative interpretation of the chemical forms of contaminant U(VI) in the vertical profile of sediments, and the development of a conceptual model that evaluates the potential release of U(VI) to the aquifer based on chemical speciation.

The kinetics of U(VI) release from these samples in artificial groundwater solutions is complex, exhibiting both fast and slow release regardless of the depth of the sample in the profile (Figs. 9, 10, 13, and 14). The U(VI) release to AGW solutions cannot be separated into contributions from desorption and dissolution processes by simplistic analysis of the kinetic data; desorption of U(VI) can be a slow process and dissolution can be fast enough to contribute to early U(VI) release. Instead, the U(VI) chemical speciation as a function of depth in the subsurface needs to be inferred from the combination of published spectroscopic results and extraction and isotopic exchange results presented in this paper.

Cu dissolution in the formate extractions (pH 3.5) illustrates clearly which samples contain U(VI) as precipitated metatorbernite. The greatest total Cu concentrations occurred in the NPP2-2, 2-4, and 2-8 samples (6.1×10^{-5}, 6.9×10^{-5}, and 1.7×10^{-5} mol/g respectively), and the greatest percentages of total Cu dissolved by the formate extraction also occurred in these samples (94, 92, and 85%, respectively, Table

4). NPP 2-4 is the sample in which Catalano et al. (2006) previously identified the occurrence of metatorbernite by spectroscopic methods. While some of the Cu dissolved in the formate extractions may have been adsorbed, the high total concentrations of Cu in these samples suggest that most of the Cu was present in precipitates. In contrast, deeper pit samples (e.g., NPP1-16, 1-20, and SPP2-16, 2-18) contained total Cu concentrations ($8.5x10^{-7}$-$1.2x10^{-6}$ mol/g) near that of background sediments, and the percentage of Cu dissolved by formate extraction was low (3-14%). The results suggest that the formate extraction was effective in dissolving contaminant Cu minerals from samples at the upper depths of the profile (including metatorbernite), and that metatorbernite was likely not present in the deep samples of the NPP1, SPP1, and SPP2 profiles, in agreement with the spectroscopic conclusions.

Catalano et al. (2006) suggested that the predominant form of uranium speciation in the deeper samples in the profile was U(VI) sorbed onto phyllosilicate minerals. Desorption of U(VI) from most mineral phases is expected to be essentially complete under the conditions of the dilute (bi)carbonate extractions (Payne et al., 1998; Kohler et al., 2004). The dilute (bi)carbonate extractions exhibited a quick release of U(VI) in the first 72 hr, followed by a slower release of U(VI) for several hundreds of hours (Fig. 4). For the deeper samples in the profiles (near or at the water table), the percentage of total U extracted in the first 72 hr ranged from 19-56% (Table 5). For these samples, it can be argued that the (bi)carbonate extraction provides a good estimate of adsorbed U(VI), because there is excellent agreement with the amount of U(VI) that undergoes isotopic exchange under artificial groundwater conditions (Table 5).

Samples that release U(VI) from both precipitated and adsorbed solid-phase speciation exhibit different behaviors. For example, for the most contaminated samples (e.g. NPP2-2, 2-4, and 2-8), there is a lack of agreement between the (bi)carbonate extraction and isotopic exchange results (Table 5), suggesting that both desorption and dissolution are contributing to U(VI) release in the (bi)carbonate extraction, and that this extraction is not useful for estimates of adsorbed U(VI) in highly contaminated samples.

The estimates of adsorbed U(VI) in each sample from the surface complexation model are in qualitative agreement with the extraction and spectroscopic results. For the samples where there was good agreement between the fraction of total U extracted by (bi)carbonate solution and undergoing isotopic exchange (samples NPP1-8, NPP1-12, NPP1-16, NPP1-20, NPP2-12, SPP1-16, SPP1-18, SPP1-22, SPP2-8, SPP2-12, SPP2-16, SPP2-18, NPP1-Fines, and SPP1-Fines), the estimates of adsorbed U(VI) by the surface complexation model were close to the values determined by (bi)carbonate extraction or isotopic exchange (Table 5). Those samples that contain metatorbernite and other U(VI) precipitates (i.e., NPP2-2 and NPP2-4) yielded estimates of adsorbed U(VI) from the surface complexation model that were much lower than that measured in (bi)carbonate extractions and isotopic exchange measurements.

The incomplete U extraction (19-55%) by the (bi)carbonate solution of the deep samples (and incomplete isotopic exchange) suggests that, in addition to adsorbed U(VI), there must be another type of uranium species in these samples. Table 3 compares the U extraction efficiencies of DCB, HH, AMOX, and formate extractions of deep vadose and groundwater fines samples, and shows that the DCB extraction was most effective at releasing U from these samples. DCB is effective at dissolving iron from crystalline

matrices, and together with the high U extraction yields of the HH and AMOX extractions, this suggests that the other type of important U chemical species for these samples is U(VI) incorporated as a co-precipitate within mineral coatings (Payne et al., 1994). The co-precipitation within coatings likely occurred after U(VI) was transported to the lower depths of the sediment profiles and concentrated by adsorption at mineral surfaces. Although mineral coatings are often described in the literature as composed of poorly crystalline phases, other studies have shown that mineral coatings containing Fe, Al, and/or Si can form nanocrystalline phases that are resistant to dissolution in the milder HH and AMOX extractions (Davis et al., 1998; Banfield and Hamers, 1998). As in the analysis of the samples containing precipitated U(VI) (Fig. 14), significant release of U(VI) from the putative co-precipitated phases would have affected the kinetics of isotopic exchange in experiments with and without long pre-equilibration times. Therefore, it appears that the U(VI) which is incorporated in the mineral coatings in the deeper vadose zone samples is relatively resistant to release to the aquifer under oxidizing conditions. The lowest yield for the DCB extraction was 67% of total U for the SPP2-18 sample, which contained only 1.2×10^{-8} mol/g U (2.9 ppm), suggesting that about 4.2×10^{-9} mol/g U (1 ppm) may be present as background U in crystalline matrices of uncontaminated Hanford silicate minerals.

While Wang et al. (2005) found U(VI) incorporation in calcite and aragonite structures in the pond bottom precipitates, U(VI)-substituted carbonate phases are likely much less abundant in the vadose samples studied here. Total carbonate in the vadose samples was <0.1% by weight, whereas pond bottom precipitates contained ~1-3% carbonate. The high levels of uranium in the pond precipitates (4.2×10^{-6} to 8.4×10^{-6}

mol/g), as well as high calcium concentrations and alkalinity, increase the likelihood that U(VI)-substituted carbonate phases formed within the pond or at the pond surface. The significant decrease in carbonate mineral content with depth suggests that carbonate minerals did not precipitate to a great extent within the vadose zone profile and have not been transported significantly as colloidal particles. In addition, Dong et al. (2005) have shown that calcite, when present, tends to actually lower U(VI) sorption in Hanford soils by blocking access to surfaces of higher sorption affinity.

5. CONCLUDING REMARKS

The combined extraction, isotopic exchange, surface complexation modeling, and previous spectroscopic results allow a more detailed conceptual model to be developed for U(VI) release to the aquifer underlying the 300 Area at Hanford and demonstrate a generic approach for evaluating chemical speciation at other contaminated sites. Few studies have been published that attempt to estimate the separate contributions of desorption and dissolution to contaminant release. Without an approach for quantifying these separate contributions, it is very difficult to develop a useful conceptual model that can be applied in reactive transport modeling for the site. Using the results presented here, it can be concluded that the more contaminated sediments located near the original pond bottoms release U(VI) primarily by dissolution of U(VI)-bearing minerals to infrequent infiltrating precipitation (Catalano et al., 2006). The released U(VI) is transported downward in the sediment profile, but the transport is retarded by adsorption to mineral coatings on the sediments. However, not all of this U(VI) appears to make it to the water table. With wet/dry cycling, a fraction of the U(VI) deeper in the sediment profiles has been sequestered as a co-precipitate into coatings that have become resistant

to dissolution as they have aged under oxidizing conditions. A fraction of sediment U(VI) near the water table is available for rapid U(VI) desorption in the capillary fringe zone, as the water table rises and falls with the variable stage of the Columbia River. The concentrations of total U in these sediments are low, but U(VI) desorption can still result in groundwater concentrations exceeding regulatory limits (for drinking water, approximately 0.1 μM). The supply of adsorbed U(VI) in the sediments near the water table is presumably replenished over time by downward U(VI) migration from the more contaminated sediments above, although the magnitude of this flux is yet to be determined. If the groundwater table rose significantly and conditions became mildly reducing, a larger reservoir of sediment U could potentially be released by dissolution of iron oxide mineral coatings.

The geochemical conceptual model described above is an obvious improvement over the constant-K_d model that has previously been applied to describe U(VI) partitioning and release from the vadose zone sediments beneath the former waste disposal ponds in the 300-Area at Hanford (Zachara et al., 2005). Although it is apparent that data obtained from chemical extractions and isotopic exchange experiments can be more meaningful when combined with spectroscopic studies of chemical speciation, few studies have applied a combination of these techniques to estimate the abundance of differing contaminant species in sediments. A better conceptual model for the site leads to a better understanding of the fundamental processes that drive U(VI) release to the aquifer, and the identification of critical fluxes in the system that need to be measured *in situ* (Davis et al., 2004b). If used carefully in combination with other methods, extractions and other types of carefully designed batch experiments can be useful

investigative tools for field sites with mixtures of adsorbed, precipitated, and co-precipitated metal contaminants.

The results have obvious relevance to the development of a better conceptual model for the 300-Area at Hanford and as input to reactive transport modeling simulations of processes occurring in the vadose zone at that site. In addition, if combined with spectroscopic studies, the experimental approach has relevance to other metal-contaminated sites where multiple processes may contribute to the overall release of contaminants to water and where the release is dependent on chemical conditions and aqueous metal speciation. In such cases, the release is poorly described by the constant K_d model or by linear sorption isotherms, which do not account for the effect of variable aqueous speciation on metal desorption or variable chemical conditions on metal dissolution.

Acknowledgements. Funding for this work was provided by an interagency agreement between the U.S. Geological Survey and Batelle Pacific Northwest National Laboratory #415428-A9E-P6490. The authors would like to thank Patricia Fox, Christopher Fuller, Matthias Kohler, and Steven Smith for technical assistance and insightful discussions.

REFERENCES

Arai, Y., Marcus, M., Tamura, Davis, J. A., and Zachara, J.M. (2007) Spectroscopic evidence for uranium bearing precipitates in vadose zone sediments at the Hanford 300-Area Site. *Environ. Sci. Technol.*, **41**, 4633-4639.

Banfield, J.F. and Hamers, R.J. (1998) Processes at minerals and surfaces with relevance to microorganisms and prebiotic synthesis: *Geomicrobiology – Interactions between Microbes and Minerals*, *Rev. Mineralogy,* **35,** 81-122.

Bernhard G., Giepel G., Reich T., Brendler V., Amayri S. and Nitshce H. (2001) Uranyl (VI) carbonate complex formation: Validation of the $Ca_2UO_2(CO_3)_3$ (aq) species. *Radiochim. Acta* **89,** 511-518.

Catalano J. G., McKinley J. P., Zachara J. M., Smith S. C., Brown G. E. (2006) Changes in uranium speciation through a depth sequence of contaminated Hanford sediments. *Environ. Sci. Technol.* **40**, 2517-2524.

Chao T. T. and Zhou L. (1983) Extraction techniques for selective dissolution of amorphous iron oxides from soils and sediments. *Soil Sci. Soc. Am. J.* **47,** 225-232.

Crowley K. D. and Ahearne J. F. (2002) Managing the environmental legacy of U.S. nuclear-weapons production. *Am. Sci.* **90,** 514-523.

Davis J. A. and Curtis G. P. (2003) Application of surface complexation modeling to describe uranium (VI) adsorption and retardation at the uranium mill tailings site at Naturita, Colorado. *NUREG/CR-6708*; U.S. Nuclear Regulatory Commission: Rockville, MD.

Davis J. A., Coston J. A., Kent D. B. and Fuller C. C. (1998) Application of the surface complexation concept to complex mineral assemblages. *Environ. Sci. Technol.* **32,** 2828.

Davis J. A. and Kent D. B. (1990) Surface complexation modeling in aqueous geochemistry: *Mineral-Water Interface Geochemistry*, *Rev. Mineralogy,* **23,** 177-260.

Davis, J. A., Payne, T. E., and Waite, T. D. (2002) Simulating the pH and pCO_2 dependence of uranium(VI) adsorption by a weathered schist with surface complexation models. In: P.-C. Zhang, & P.V. Brady (Eds). *Geochemistry of Soil Radionuclides (Special Publication Number 59)*, Soil Science Society of America, Madison, WI, p. 61-86.

Davis J. A., Meece D. E., Kohler M. and Curtis G. P. (2004a) Approaches to surface complexation modeling of uranium(VI) adsorption on aquifer sediments. *Geochim. Cosmochim. Acta* **68,** 3621-3641.

Davis, J. A. Yabusaki S. B., Steefel C. I., Zachara J. M., Curtis G. P., Redden G. D., Criscenti L. J., and Honeyman B. D. (2004b) *EOS*, Assessing conceptual models for subsurface reactive transport of inorganic contaminants, **85**, 449-455.

Dong W, Ball W. P., Liu C., Wang Z., Stone A. T., Bai J., and Zachara J. M. (2005) Influence of calcite and dissolved calcium on uranium(VI) sorption to a Hanford subsurface sediment. *Environ. Sci. Technol.* **39,** 7949 -7955.

Dove P. M. and Hochella M. F. J. (1993) Calcite precipitation mechanisms and inhibition by orthophosphate: In situ observations by scanning force microscopy. *Geochim. Cosmochim. Acta* **57,** 705-714.

Fox P. M., Davis J. A. and Zachara J. M. (2006) The effect of calcium on aqueous uranium(VI) speciation and adsorption to ferrihydrite and quartz. *Geochim. Cosmochim. Acta* **70,** 1379-1387.

Guillaumont R., Fanghanel T., Neck V., Fuger J., Palmer D. A., Grenthe I. and Rand M. H. (2003) *Update on the Chemical Thermodynamics of Uranium, Neptunium, Plutonium, Americium, and Technetium.* Elsevier, Amsterdam.

Herbelin A. L. and Westall J. C. (1999) *FITEQL: A Computer Program for the Determination of Chemical Equilibrium Constants from Experimental Data.* Chemistry Department, Oregon State University, Corvallis, Oregon.

Inskeep W. P. and Bloom P. R. (1986) Kinetics of calcite precipitation in the presence of water soluble organic ligands. *Soil Sci. Soc. Amer. J.* **50,** 1167-1172.

Kalmykov N. and Choppin G. R. (2000) Mixed $Ca^{2+}/UO_2^{2+}/CO_3^{2-}$ complex formation at different ionic strengths. *Radiochim. Acta* **88,** 603-606.

Kohler M., Curtis G. P., Meece D. E. and Davis J. A. (2004) Methods for estimating adsorbed uranium(VI) and distribution coefficients of contaminated sediments. *Environ. Sci. Technol.* **38,** 240-247.

Lebron I. and Suarez D. L. (1996) Calcite nucleation and precipitation kinetics as affected by dissolved organic matter at 25^{o}C and pH > 7.5. *Geochim. Cosmochim. Acta* **60,** 2765-2776.

Lindberg J. W. and Peterson R. E. (2004) 300-FF-5 Operable Unit. In *Hanford Site Groundwater Monitoring for Fiscal Year 2004* (eds. M. J. Hartman, L. F. Morasch, and W. D. Webber). Pacific Northwest National Laboratory, Richland, Washington. PNNL-15070. pp 2.12-1-2.12-31.

Meece D. E. and Benninger L. K. (1993) The coprecipitation of Pu and other radionuclides with $CaCO_3$. *Geochim. Cosmochim. Acta* **57,** 1447-1458.

Nielson K. K. (1978) Application of direct peak analysis to energy-dispersive X-Ray fluorescence spectra. *X-Ray Spect.* **7,** 15-22.

Payne T. E., Lumpkin G. R. and Waite T. D. (1998) Uranium(VI) adsorption on model minerals: Controlling factors and surface complexation modeling. In *Adsorption of Metals by Geomedia* (eds. E. A. Jenne). Academic Press, San Diego, CA. pp. 75-97.

Payne T. E., Davis J. A., and Waite T. D. (1994) Uranium retention by weathered schists - The role of iron minerals. *Radiochim. Acta* **66/67**, 297-303.

Qafoku N. P., Zachara J. M., Liu C., Gassman P. L., Qafoku O. S. and Smith S. C. (2005) Kinetic desorption and sorption of U(VI) during reactive transport in a contaminated Hanford sediment. *Environ. Sci. Technol.* **39,** 3157-3165.

Reddy M. M. and Wang K. K. (1973) Calcite crystal growth inhibition by phosphates. *Desalination* **12,** 61-73.

Reeder R. J., Nugent M., Tait C. D., Morris D. E., Heald S. M., Beck K. M., Hess W. P. and Lanzirotti A. (2001) Coprecipitation of uranium(VI) with calcite: XAFS, micro-XAS, and luminescence characterization. *Geochim. Cosmochim. Acta* **65,** 3491-3503.

Riley R.G., Zachara, J. M., and Wobber, F. J. (1992) Chemical contaminants on DOE lands and selection of contaminant mixtures for subsurface science research. United States Department of Energy, Subsurface Science Program, Washington, DC. DOE/ER--0547T.

Serne R. J., Brown C. B., Schaef H. T., Pierce E. M., Lindberg M. J., Wang Z., Gassman P. and Catalano J. (2003) 300 Area uranium leach and adsorption project. U.S. Department of Energy, Washington, D.C. PNNL-14022.

Turner G. D., Zachara J. M., McKinley J. P. and Smith S. C. (1996) Surface-charge properties and UO_2^{2+} adsorption of a subsurface smectite. *Geochim. Cosmochim. Acta* **60,** 3399-3414.

USDOE. (2005) Work plan for Phase III feasibility study 300-FF-5 operable unit. United States Department of Energy, Richland, Washington. DOE/RL-2005-41.

USEPA. (1996) Record of Decision for the Hanford 300-Area Site. Environmental Protection Agency, Washington, D.C. EPA/ROD/R10-96/143.

Wang Z., Zachara J. M., McKinley J. P., Smith S. C. and Heald S. M. (2005) Cryogenic laser induced U(VI) fluorescence studies of a U(VI) substituted natural calcite: Implications to U(VI) speciation in contaminated Hanford sediments. *Environ. Sci. Technol.* **39,** 2651-2659.

Wang Z., Zachara J. M., Yantasee W., Gassman P.L., Liu C., Joly A.G. (2004) Cryogenic laser induced U(VI) fluorescence characterization of U(VI) in Hanford vadose zone pore waters. *Environ. Sci. Technol.* **38,** 5591-5597.

Zachara J. M., Davis J. A., Liu C., McKinley J. P., Qafoku N., Wellman D. M., Yabusaki S. (2005) Uranium geochemistry in vadose zone and aquifer sediments from the 300 Area uranium plume. U.S. Department of Energy, Washington, D.C. PNNL-15121.

Table 1. Composition of Artificial Groundwaters (elemental concentration in mmol/L), $pCO_2 = 10^{-3.5}$

AGW	Ca^{2+}	Mg^{2+}	K^+	Na^+	HCO_3^-	SO_4^{2-}	NO_3^-	Alk. (meq/L)	Ionic Strength	Initial pH
2	0.6	0.2	0.1	15	10	1.8	3.0	10	19.3	8.30
3	0.6	0.2	0.1	7.0	2.0	1.8	3.0	2.0	11.3	8.40
4	0.6	0.1	0.1	8.0	4.0	1.2	3.0	4.0	11.4	8.65
5	0.6	0.4	0.5	6.0	1.0	2.0	3.5	1.0	11.4	8.07
6	0.6	0.5	0.5	5.5	0.5	2.1	3.5	0.5	11.4	7.85
8	0.6	0.2	0.1	97	2.0	1.8	93	2.0	101	8.26
9	0.6	0.1	0.1	98	4.0	1.2	93	4.0	101	8.30
10	0.6	0.4	0.5	96	1.0	2.0	94	1.0	102	8.12
11	0.6	0.5	0.5	96	0.5	2.1	94	0.5	101	8.05
12	0.6	0.1	0.1	8.4	6.0	0.9	2.1	6.0	11.5	8.59
13	0.6	0.5	0.2	8.9	8.0	0.8	1.7	8.0	13.2	8.55

Table 2. Formation Constants for U(VI) Solution Species

Reaction	log K (I = 0)[a]
$UO_2^{2+} + H_2O \Leftrightarrow UO_2OH^+ + H^+$	-5.25
$UO_2^{2+} + 2H_2O \Leftrightarrow UO_2(OH)_{2,aq} + 2H^+$	-12.15
$UO_2^{2+} + 3H_2O \Leftrightarrow UO_2(OH)_3^- + 3H^+$	-20.25
$UO_2^{2+} + 4H_2O \Leftrightarrow UO_2(OH)_4^{2-} + 4H^+$	-32.4
$2UO_2^{2+} + H_2O \Leftrightarrow (UO_2)_2OH^{3+} + H^+$	-2.70
$2UO_2^{2+} + 2H_2O \Leftrightarrow (UO_2)_2(OH)_2^{2+} + 2H^+$	-5.62
$3UO_2^{2+} + 4H_2O \Leftrightarrow (UO_2)_3(OH)_4^{2+} + 4H^+$	-11.90
$3UO_2^{2+} + 5H_2O \Leftrightarrow (UO_2)_3(OH)_5^+ + 5H^+$	-15.55
$3UO_2^{2+} + 7H_2O \Leftrightarrow (UO_2)_3(OH)_7^- + 7H^+$	-32.20
$4UO_2^{2+} + 7H_2O \Leftrightarrow (UO_2)_4(OH)_7^+ + 7H^+$	-21.9
$UO_2^{2+} + CO_3^{2-} \Leftrightarrow UO_2CO_3(aq)$	9.94
$UO_2^{2+} + 2CO_3^{2-} \Leftrightarrow UO_2(CO_3)_2^{2-}$	16.61
$UO_2^{2+} + 3CO_3^{2-} \Leftrightarrow UO_2(CO_3)_3^{4-}$	21.84
$2UO_2^{2+} + CO_3^{2-} + 3H_2O \Leftrightarrow (UO_2)_2CO_3(OH)_3^- + 3H^+$	-0.855
$Ca^{2+} + UO_2^{2+} + 3CO_3^{2-} \Leftrightarrow CaUO_2(CO_3)_3^{2-}$	25.64 [b]
$2Ca^{2+} + UO_2^{2+} + 3CO_3^{2-} \Leftrightarrow Ca_2UO_2(CO_3)_3$ (aq)	30.04 [c]
$UO_2^{2+} + NO_3^- \Leftrightarrow UO_2NO_3^+$	0.3
$UO_2^{2+} + Cl^- \Leftrightarrow UO_2Cl^+$	0.17
$UO_2^{2+} + 2Cl^- \Leftrightarrow UO_2Cl_2(aq)$	-1.1
$UO_2^{2+} + SO_4^{2-} \Leftrightarrow UO_2SO_4(aq)$	3.15
$UO_2^{2+} + 2SO_4^{2-} \Leftrightarrow UO_2(SO_4)_2^{2-}$	4.14

[a] Values from Guillaumont et al. (2003), unless otherwise indicated.

[b] Bernhard et al. (2001), with correction to be consistent with Guillaumont et al. (2003).

[c] Kalmykov and Choppin (2000), with correction to be consistent with Guillaumont et al. (2003).

Table 3. Iron (μmol/g) and uranium (% of total U) removed in various extractions*.

Sample	DCB Fe (μmol/g) [a]	HH Fe (μmol/g) [b]	AMOX Fe (μmol/g) [c]	DCB % of U_{tot} [a,d]	HH % of U_{tot} [b,d]	AMOX % of U_{tot} [c,d]
NPP 1-16	158	41	91	100	92.2	81.7
NPP 1-20	142	46	95	100	75.6	74.7
SPP 2-16	151	--	88	90.5	--	73.0
SPP 2-18	77	19	48	66.7	58.3	50.0
NPP 1-Fines	296	102	108	100	96.6	94.4
NPP 2-Fines	224	90	89	104	109	114
SPP 1-Fines	239	90	86	99.2	91.6	91.6
SPP 2-Fines	232	83	70	96.6	91.2	87.7

* Values are the mean of two replicates, error based on replicate variation.

[a] DCB refers to dithionite citrate bicarbonate extractions

[b] HH refers to hydroxylamine hydrochloride extraction for 0.5 hr (dissolves poorly crystalline minerals)

[c] AMOX refers to ammonium oxalate extraction (dissolves poorly crystalline iron oxyhydroxides)

[d] % of U_{tot} refers to percentage of total uranium dissolved by each extraction method

Table 4. Total Uranium and U/Cu Extracted by Sodium Formate (nanomoles/g)*

Sample	Surface Area (m^2/g)	Total U Measured by Gamma-Spectrometry [a]	[U(VI)] Extracted by Formate [b]	Total [Cu] Measured by XRF [c]	[Cu] Extracted by Formate [b]
NPP 1-8	19.9 ± 0.04	44.0 ± 3.2	44.7 ± 1.4	985 ± 110	72.9 ± 2.7
NPP 1-12	27.2 ± 0.05	58.9 ± 4.2	53.2 ± 1.8	1210 ± 120	78.8 ± 8.0
NPP 1-16	27.2 ± 0.01	40.4 ± 3.2	33.3 ± 1.1	1170 ± 120	123 ± 3.5
NPP 1-20	17.5 ± 0.06	26.3 ± 2.1	20.4 ± 0.65	1090 ± 110	151 ± 13
NPP 2-2	17.8 ± 0.23	444 ± 24	322 ± 5.8	64800 ± 3300	61000 ± 4.4
NPP 2-4	21.8 ± 0.03	421 ± 21	344 ± 6.8	75500 ± 3800	69100 ± 3500
NPP 2-8	18.5 ± 0.04	167 ± 10	114 ± 3.3	20200 ± 1000	17100 ± 360
NPP 2-12	14.7 ± 0.05	59.7 ± 3.5	63.9 ± 0.73	1770 ± 140	784 ± 36
SPP 1-16	21.2 ± 0.04	30.8 ± 2.4	31.4 ± 1.0	877 ± 120	34.3 ± 0.44
SPP 1-18	22.0 ± 0.09	31.2 ± 2.8	24.5 ± 0.77	897 ± 120	34.6 ± 0.44
SPP 1-22	25.8 ± 0.63	33.0 ± 2.4	22.7 ± 0.73	815 ± 100	14.6 ± 0.90
SPP 2-8	17.7 ± 0.11	45.3 ± 2.6	41.5 ± 1.3	903 ± 120	31.2 ± 4.5
SPP 2-12	15.9 ± 0.04	33.5 ± 2.7	33.5 ± 1.1	721 ± 98	18.2 ± 1.3
SPP 2-16	15.5 ± 0.05	16.2 ± 1.6	15.1 ± 0.45	845 ± 98	28.4 ± 0.59
SPP 2-18	15.3 ± 0.19	12.0 ± 1.5	7.28 ± 0.23	895 ± 98	40.1 ± 1.8
NPP 1-Fines	46.9 ± 2.3	89.0 ± 5.2	69.7 ± 0.79	2660 ± 160	314 ± 0.43
NPP 2-Fines	N/A	660 ± 34	N/A	43000 ± 2200	N/A
SPP 1-Fines	53.9 ± 2.7	131 ± 7.2	103 ± 1.2	1520 ± 130	215 ± 3.6
SPP 2-Fines	40.5 ± 2.0	55.9 ± 3.7	42.4 ± 1.4	1330 ± 100	102 ± 0.89

* Values are the mean of two replicates, error based on replicate variation.

[a] Sum of ^{238}U and ^{235}U

[b] Formate extraction (72 hr)

[c] Total copper measured by X-ray fluorescence spectroscopy (XRF). Data collection and analyses by Steven Smith, PNNL.

Table 5. Fractional dissolution of uranium in extractions, fraction of total U exchanged in isotopic exchange experiments, and model-estimated fraction of total U present as adsorbed U(VI)[*].

Sample	Total U (ppm) [a]	Formate Extraction % of U_{tot} [b]	Bicarbonate Extraction % of U_{tot} [c]	Isotopic Exchange % of U_{tot} [d]	Estimate of Adsorbed U(VI) % of U_{tot} [e]
NPP 1-8	10.5	101.5 ± 3.2	45.0 ± 0.2	46.0 ± 3.3	54
NPP 1-12	14.0	90.3 ± 3.1	42.7 ± 1.0	44.7 ± 3.6	61
NPP 1-16	9.6	82.5 ± 2.7	38.3 ± 3.3	44.6 ± 1.9	57
NPP 1-20	6.3	77.5 ± 2.5	29.7 ± 0.45	35.8 ± 0.70	41
NPP 2-2	105.7	72.5 ± 1.3	29.8 ± 2.8	46.4 ± 2.2	18
NPP 2-4	100.1	79.6 ± 1.6	29.4 ± 1.3	88.2 ± 8.6	13
NPP 2-8	39.8	68.3 ± 2.0	37.6 ± 1.1	56.3 ± 2.5	45
NPP 2-12	14.2	107.1 ± 1.2	56.1 ± 1.8	61.2 ± 2.0	70
SPP 1-16	7.3	101.9 ± 3.2	54.7 ± 0.99	55.1 ± 2.5	55
SPP 1-18	7.4	78.5 ± 2.5	36.0 ± 0.97	35.8 ± 0.74	28
SPP 1-22	7.9	68.9 ± 2.2	35.4 ± 0.08	37.1 ± 1.4	29
SPP 2-8	10.8	91.6 ± 2.9	43.8 ± 2.5	44.7 ± 4.9	52
SPP 2-12	8.0	100.1 ± 3.3	57.6 ± 1.2	54.7 ± 2.7	61
SPP 2-16	3.8	93.1 ± 2.8	41.0 ± 1.9	42.2 ± 4.0	34
SPP 2-18	2.9	61.0 ± 1.9	18.9 ± 1.3	21.1 ± 0.3	15
NPP 1-Fines	21.2	78.3 ± 0.89	41.4 ± 0.77	47.7 ± 2.1	57
NPP 2-Fines	157.1	--	41.4 ± 1.5	--	--
SPP 1-Fines	31.3	78.7 ± 0.89	58.0 ± 0.13	56.1 ± 7.0	66
SPP 2-Fines	13.3	75.8 ± 2.6	39.9 ± 0.68	52.6 ± 1.0	38

[*] Values are the mean of two replicates, error based on replicate variation.

[a] Sum of ^{238}U and ^{235}U (Uranium concentration in nmoles/g are listed in Table 4)

[b] Formate extraction (72 hr)

[c] Bicarbonate extraction, pH 9.45 (72 hr)

[d] Isotopic exchange, 336 hr (after 1260 hr pre-equilibration in AGW4).

[e] Estimate of adsorbed U(VI) in each sample from the semi-mechanistic surface complexation model calibrated with deep vadose zone samples. Adsorbed U(VI) in the sample calculated with the model by estimation of dissolved U(VI) concentration that would result from desorption after 96 hr equilibration in AGW4 (see text).

Table 6. U(VI) Surface Reactions Considered for the Generalized Composite SCM

Number	Reaction
1	$SOH + UO_2^{2+} = SOUO_2^{+} + H^{+}$
2	$SOH + UO_2^{2+} + H_2O = SOUO_2OH + 2H^{+}$
3	$SOH + UO_2^{2+} + H_2CO_3 = SOUO_2HCO_3 + 2H^{+}$
4	$SOH + UO_2^{2+} + H_2CO_3 = SOUO_2CO_3^{-} + 3H^{+}$
5	$SOH + UO_2^{2+} + H_2CO_3 + H_2O = SOUO_2OHCO_3^{2-} + 4H^{+}$
6	$SOH + UO_2^{2+} + 2H_2CO_3 = SOUO_2(HCO_3)_2^{-} + 3H^{+}$
7	$SOH + UO_2^{2+} + 2H_2CO_3 = SOUO_2(CO_3HCO_3)^{2-} + 4H^{+}$
8	$SOH + UO_2^{2+} + 2H_2CO_3 = SOUO_2(CO_3)_2^{3-} + 5H^{+}$
9	$SOH + UO_2^{2+} + 2H_2CO_3 + H_2O = SOUO_2OH(CO_3)_2^{4-} + 6H^{+}$

Table 7. Surface Complexation Model Parameters

U(VI) Surface Reaction [1]	Log K_f (I=0)
Average Model based on all data	
$SOH + UO_2^{2+} + H_2O = SOUO_2OH + 2H^{+}$	-5.152
$SOH + UO_2^{2+} + H_2CO_3 = SOHUO_2CO_3 + 2H^{+}$	-0.833
NPP Sediment Model	
$SOH + UO_2^{2+} + H_2O = SOUO_2OH + 2H^{+}$	-4.722
$SOH + UO_2^{2+} + H_2CO_3 = SOHUO_2CO_3 + 2H^{+}$	-0.895
SPP Sediment Model	
$SOH + UO_2^{2+} + H_2O = SOUO_2OH + 2H^{+}$	-5.235
$SOH + UO_2^{2+} + H_2CO_3 = SOHUO_2CO_3 + 2H^{+}$	-1.033

[1] Total site concentration equal to 3.84 μmoles/m^2 of sediment surface area.

Figure Captions

Fig. 1. Map of 300-Area at Hanford, showing the locations of the North and South Process Pond pits. Contour lines indicate U(VI) concentrations in the groundwater plume beneath the 300-Area in December 2002.

Fig. 2. Conceptual diagram of a depth profile within a pit at the 300-Area showing U(VI) speciation from previous spectroscopic studies.

Fig. 3. Depth sequence profiles of the four sampling pits in the North and South Process Ponds of the 300-Area at Hanford. Sample depth below excavated (or secondary) pond surface is shown along with U concentrations. Seasonal water table variation is also shown. Note different scales for total U concentrations in the sediments. 1 ppm U = 4.2 nmol/g U.

Fig. 4. Uranium(VI) and calcium concentrations during a dilute (bi)carbonate extraction of sediment sample, NPP1-16 (50 g/L). Note log scale on x-axis. Values are the mean of two replicates. Error bars based on replicate variation for all Figures.

Fig. 5. Aqueous concentrations of selected elements during reaction of artificial groundwater solution 4 with sediment sample, NPP1-16 (100 g/L). Concentrations of Ca and Na(x0.1) are plotted on the left y-axis. All other elements are shown on the right y-axis. Note log scale on x-axis.

Fig. 6. Measured alkalinity as a function of reaction time of sample NPP1-20 (200 g/L) in artificial groundwater solutions with variable bicarbonate concentrations.

Fig. 7. Calcite saturation index versus alkalinity in batch reactions of artificial groundwater solutions with selected NPP and SPP sediment samples for 96 hr.

Saturation index of calcite was calculated from FITEQL-calculated aqueous speciation using the formula: SI = (Log IAP, ion activity product) - (-8.48, the log of the solubility product).

Fig. 8. Calculated aqueous speciation of a 2 μM U(VI) solution at pH 7.87 and at equilibrium with calcite as a function of alkalinity. Total alkalinity was assumed to be due to bicarbonate and carbonate alkalinity only.

Fig. 9. U(VI) desorption from various samples (200 g/L) during reaction with AGW 4 (4 meq/L).

Fig. 10. U(VI) desorption from sediment sample, NPP1-16 (200 g/L), during reaction with artificial groundwater solutions of varying alkalinity. AGW2, alkalinity = 9 meq/L; AGW4 = 4 meq/L; AGW3 = 2 meq/L; AGW5 = 1 meq/L. Total adsorbed U(VI) for the sample was estimated from the amount of labile U(VI) determined in 336-hr isotopic exchange experiments.

Fig. 11. U(VI) released from various samples (200 g/L) after 72 hr of reaction in artificial groundwater solutions with variable alkalinity.

Fig. 12. U(VI) desorbed from sample, NPP1-16, after 72 hr reaction at variable solid:water ratios in AGW4 (I = 0.01 M) and AGW9 (I = 0.1 M).

Fig. 13. Dissolved U(VI) concentration, ^{233}U activity in solution, and calculated labile U(VI) from isotopic exchange experiments conducted in AGW4 with sediment sample, NPP1-16 (100 g/L), with a) 24 hr pre-equilibration time, and b) 1260 hr pre-equilibration time.

Fig. 14. Dissolved U(VI) concentration, ^{233}U activity in solution, and calculated labile U(VI) from isotopic exchange experiments conducted in AGW4 with sediment

sample, NPP2-4, with a) 24 hr pre-equilibration time (100 g/L), and b) 1260 hr pre-equilibration time (30 g/L).

Fig. 15. Uranium(VI) adsorption isotherms for deeper pit sediment samples suspended in AGW4 or AGW9. Alkalinities in the NPP experiments ranged from 164 to 227 mg/L as $CaCO_3$ (average of 188 mg/L), causing some of the scatter in the data. Alkalinities in the SPP experiments ranged from 168 to 226 mg/L (average of 190 mg/L). Solid curves show the fits to the data with surface complexation models calibrated with all of the data, or separately with NPP or SPP sediment data.

Fig. 16. Alkalinity dependence of log K_d values for U(VI) sorption for deeper pit sediment samples equilibrated in artificial groundwater solutions of varying composition. Solid curves show the fits to the data with surface complexation models calibrated with all of the data, or separately with NPP or SPP sediment data.

Figure 1.

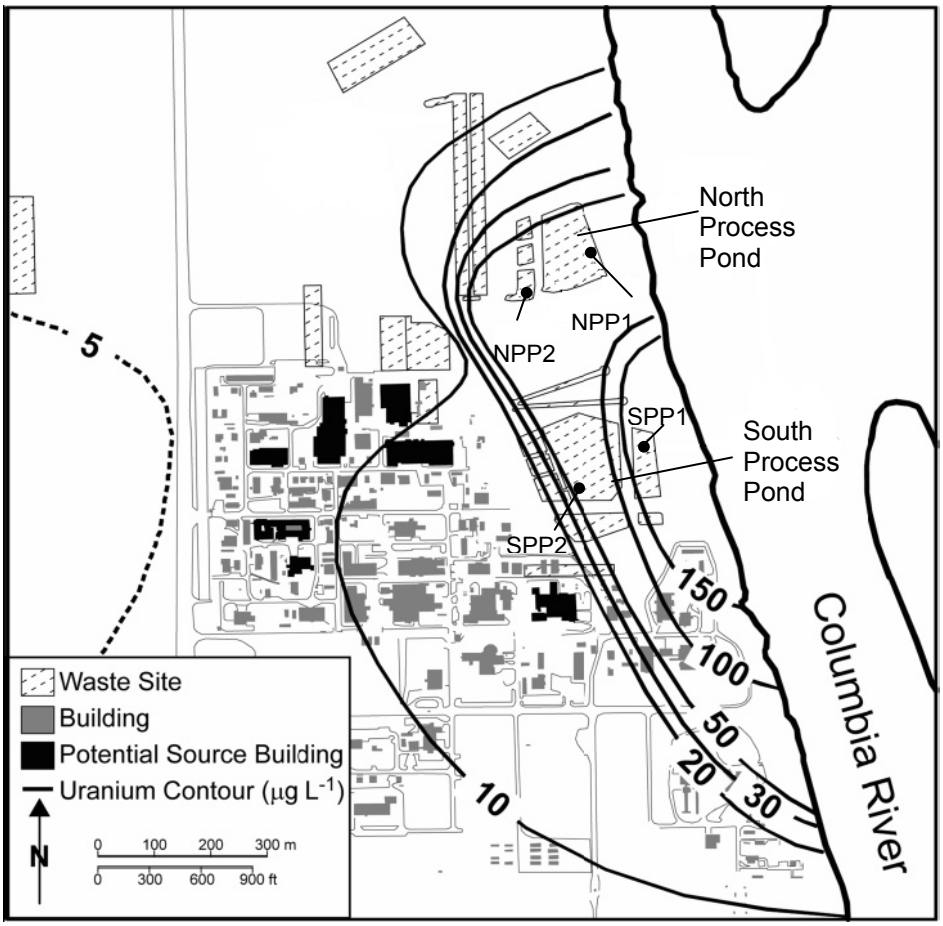
North
Process
Pond
NPP1
NPP2
SPP1
South
Process
Pond
SPP2
5
150
100
50
20
30
10
Columbia River
Waste Site
Building
Potential Source Building
Uranium Contour (μg L-1)
N
0 100 200 300 m
0 300 600 900 ft

Figure 2.

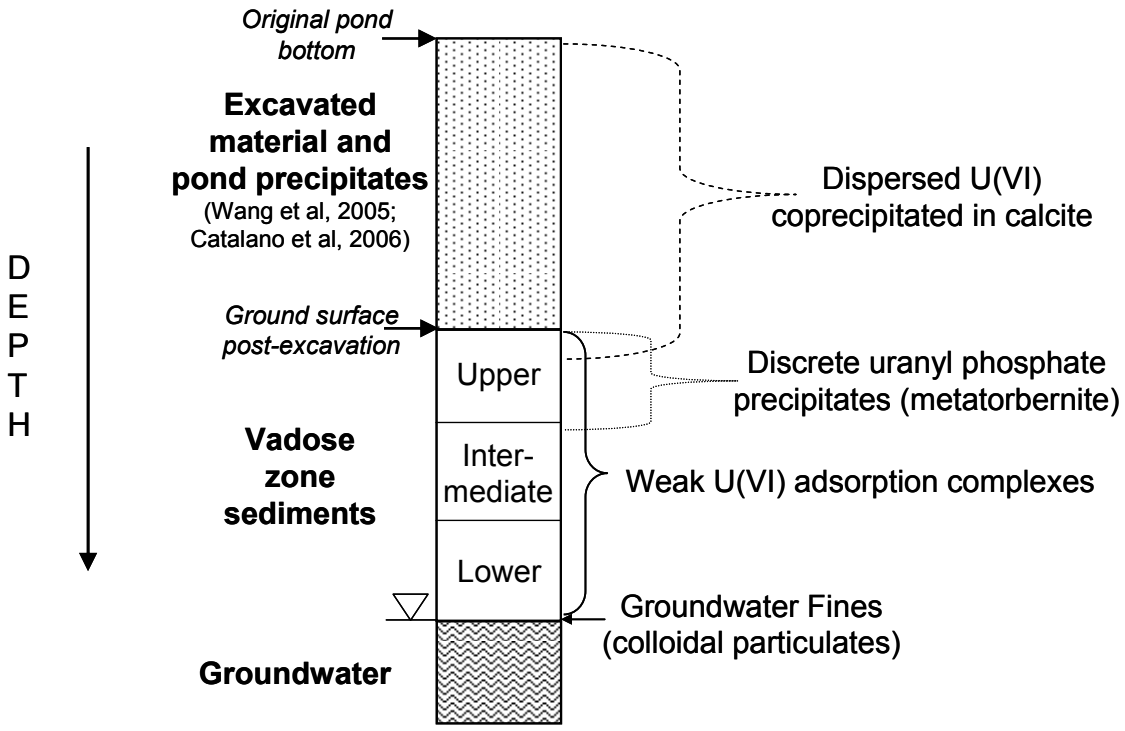
Original pond bottom
Excavated material and pond precipitates
(Wang et al, 2005; Catalano et al, 2006)
Ground surface post-excavation
Upper
Inter-mediate
Lower
Vadose zone sediments
Groundwater
DEPTH
Dispersed U(VI) coprecipitated in calcite
Discrete uranyl phosphate precipitates (metatorbernite)
Weak U(VI) adsorption complexes
Groundwater Fines (colloidal particulates)

Figure 3.

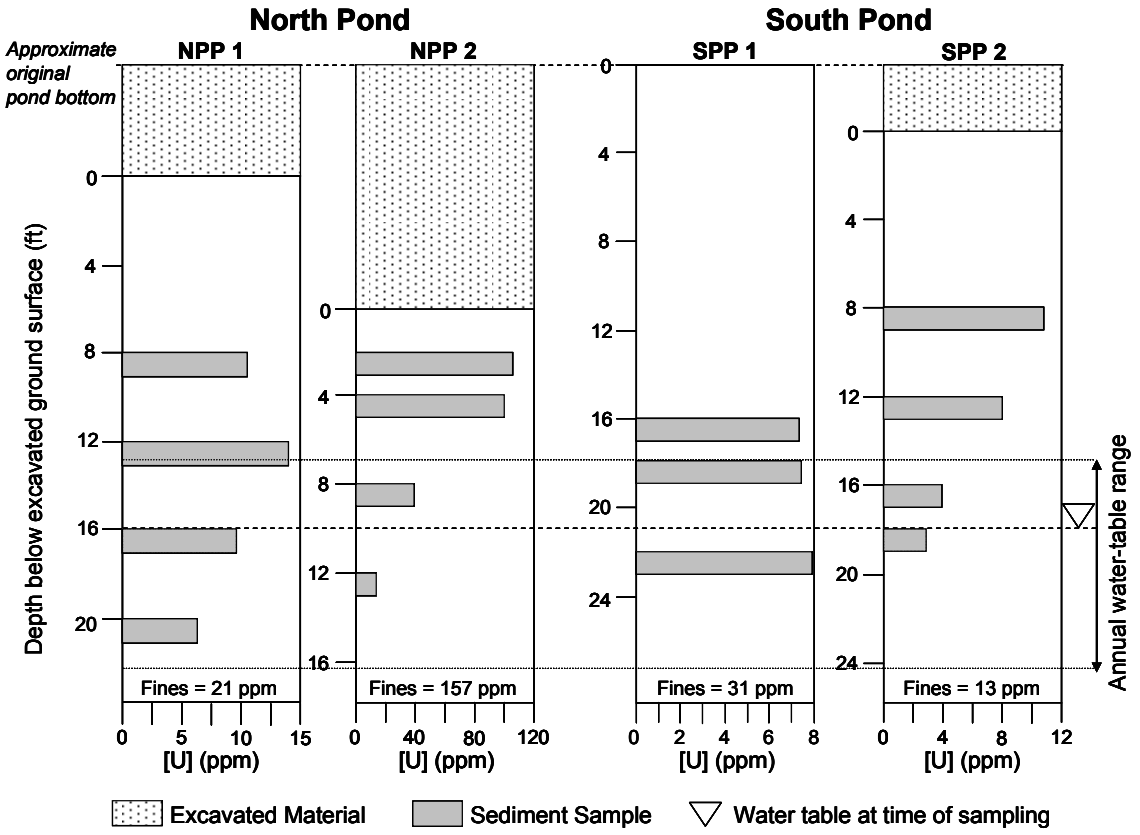
North Pond
South Pond
Approximate original pond bottom
NPP 1
NPP 2
SPP 1
SPP 2
Depth below excavated ground surface (ft)
Annual water-table range
Fines = 21 ppm
Fines = 157 ppm
Fines = 31 ppm
Fines = 13 ppm
[U] (ppm)
Excavated Material
Sediment Sample
Water table at time of sampling

Figure 4.

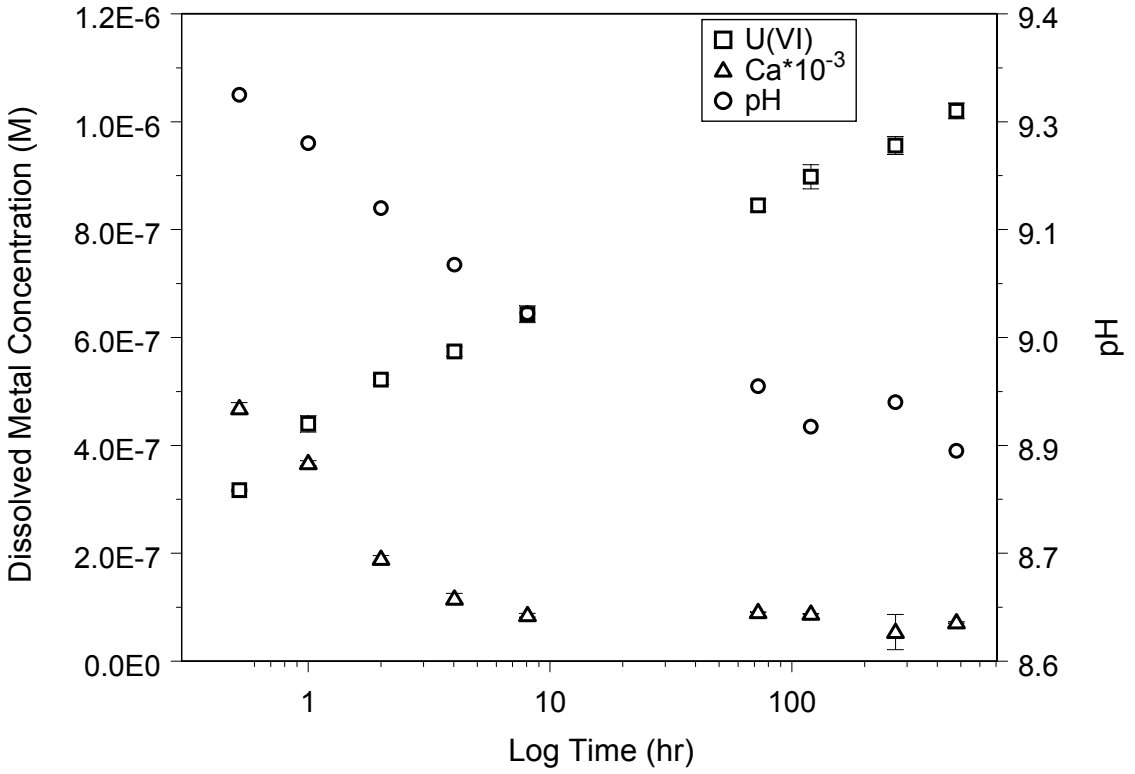
U(VI)
Ca*10-3
pH
Dissolved Metal Concentration (M)
1.2E-6
1.0E-6
8.0E-7
6.0E-7
4.0E-7
2.0E-7
0.0E0
9.4
9.3
9.1
9.0
8.9
8.7
8.6
pH
1
10
100
Log Time (hr)

Figure 5.

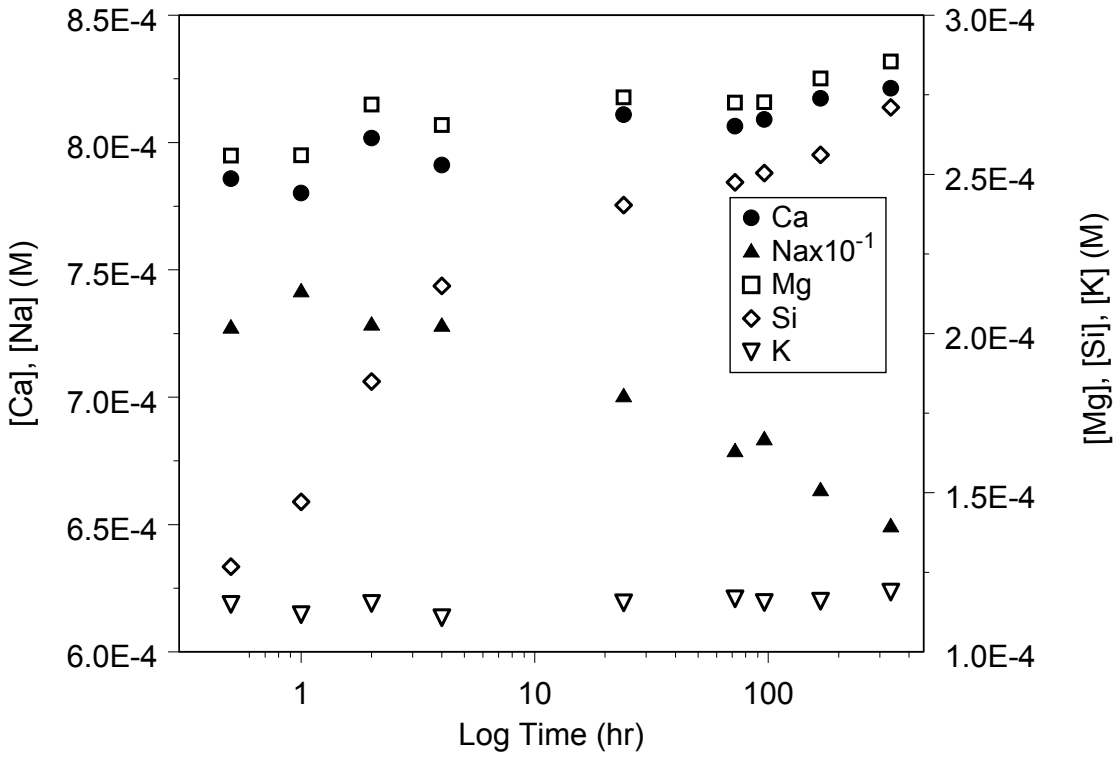
8.5E-4
8.0E-4
7.5E-4
7.0E-4
6.5E-4
6.0E-4
[Ca], [Na] (M)
3.0E-4
2.5E-4
2.0E-4
1.5E-4
1.0E-4
[Mg], [Si], [K] (M)
1
10
100
Log Time (hr)
Ca
Nax10-1
Mg
Si
K

Figure 6.

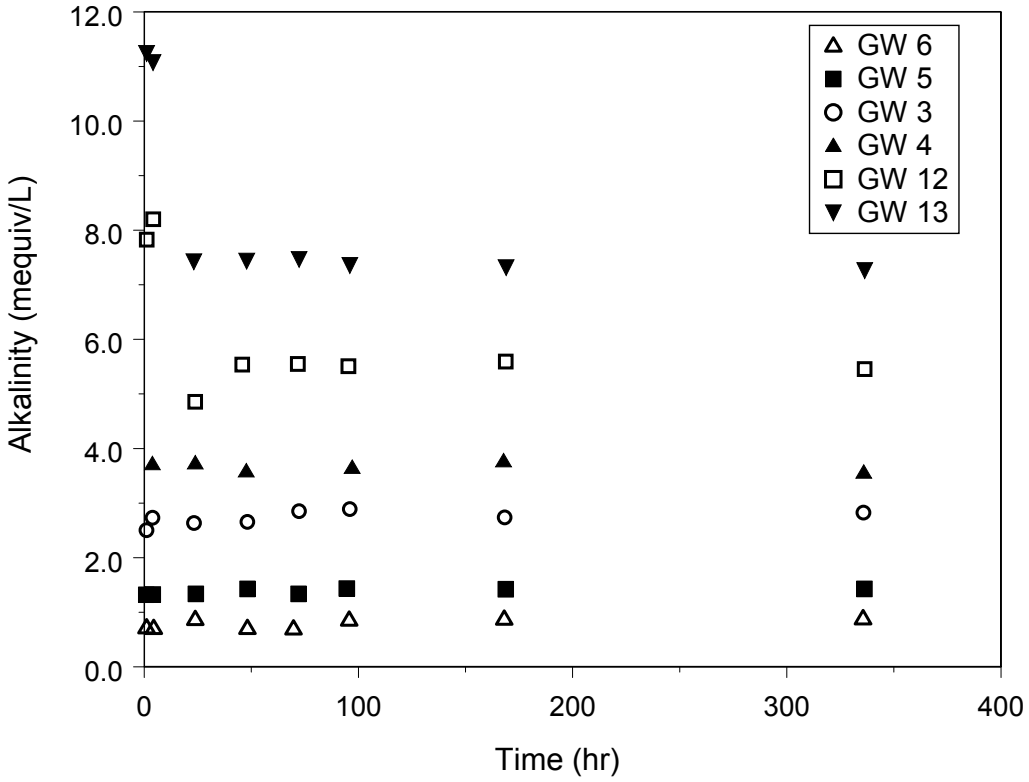
12.0
10.0
8.0
6.0
4.0
2.0
0.0
Alkalinity (mequiv/L)
0
100
200
300
400
Time (hr)
GW 6
GW 5
GW 3
GW 4
GW 12
GW 13

Figure 7.

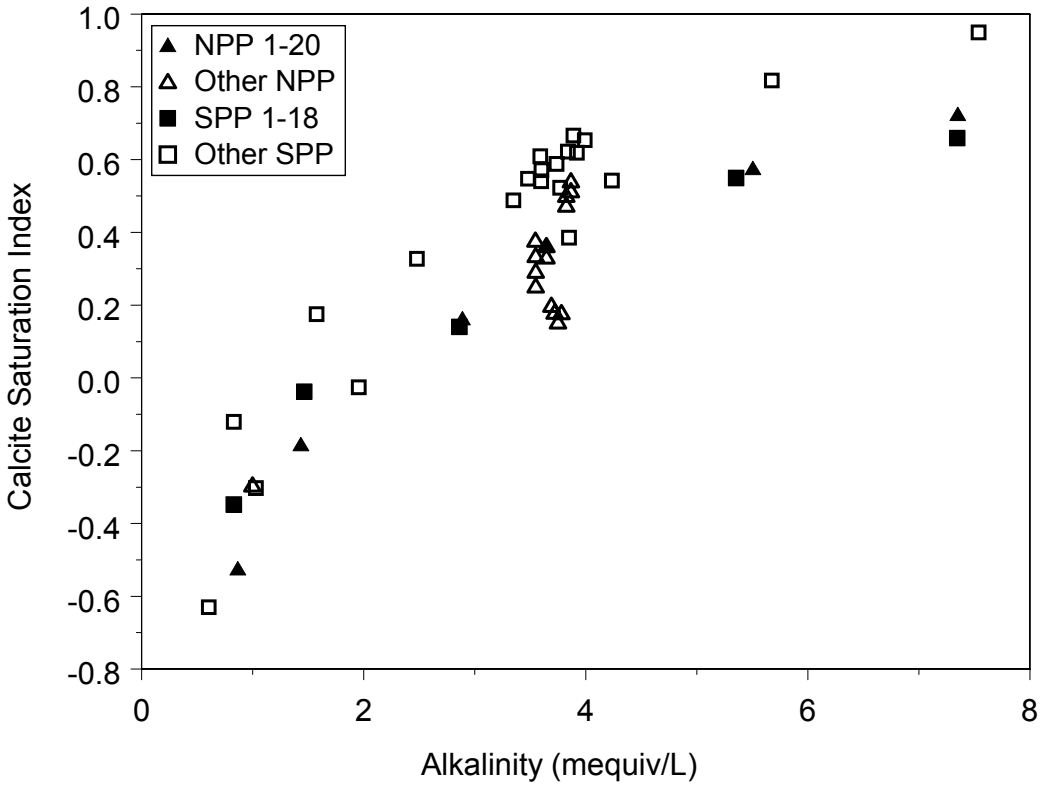
NPP 1-20
Other NPP
SPP 1-18
Other SPP
Calcite Saturation Index
Alkalinity (mequiv/L)
1.0
0.8
0.6
0.4
0.2
0.0
-0.2
-0.4
-0.6
-0.8
0
2
4
6
8

Figure 8.

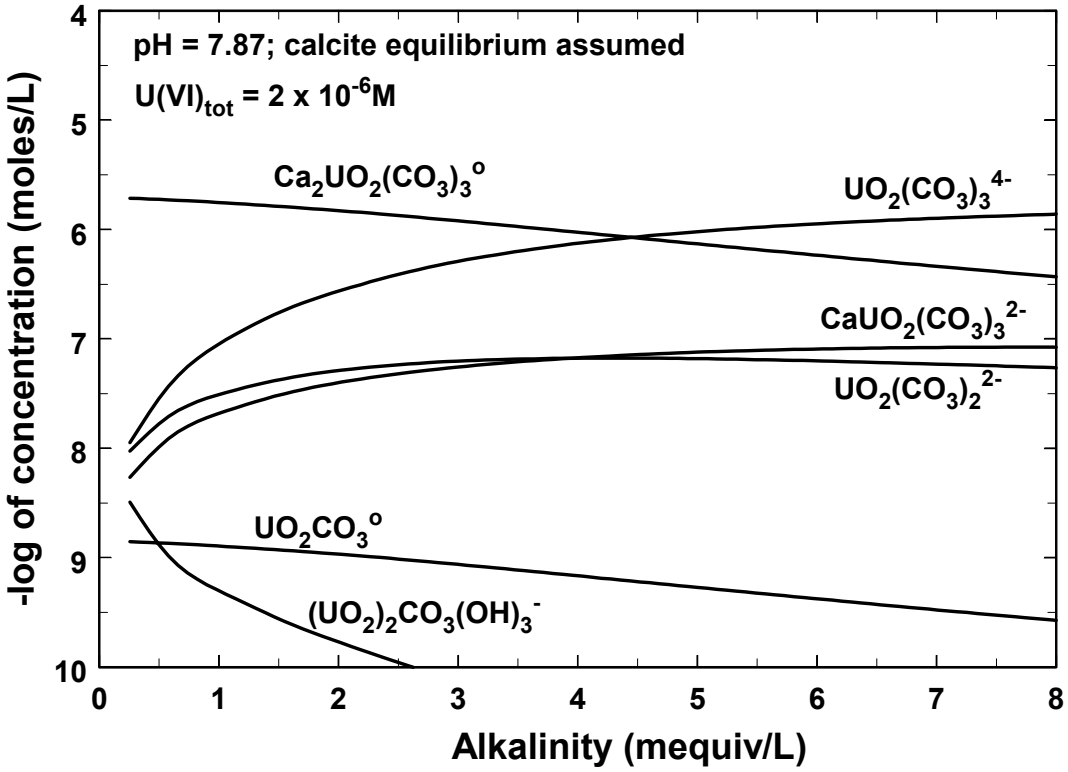
pH = 7.87; calcite equilibrium assumed
U(VI)tot = 2 x 10-6M
Ca2UO2(CO3)3o
UO2(CO3)34-
CaUO2(CO3)32-
UO2(CO3)22-
UO2CO3o
(UO2)2CO3(OH)3-
-log of concentration (moles/L)
Alkalinity (mequiv/L)
4
5
6
7
8
9
10
0
1
2
3
4
5
6
7
8

Figure 9.

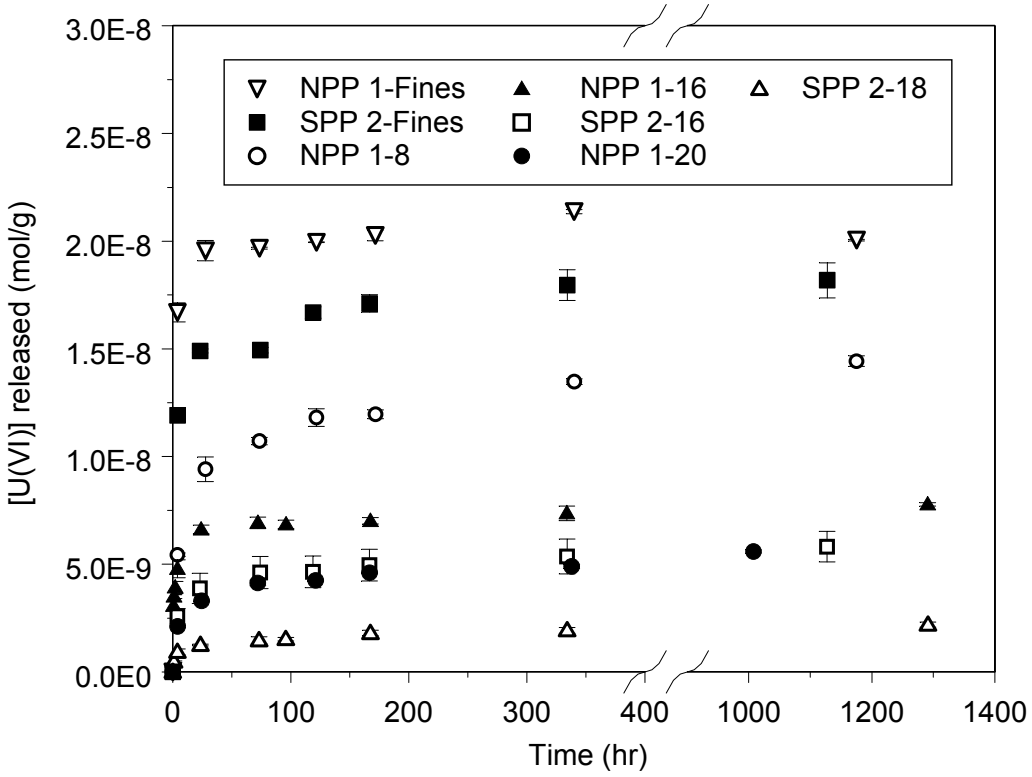
3.0E-8
2.5E-8
2.0E-8
1.5E-8
1.0E-8
5.0E-9
0.0E0
[U(VI)] released (mol/g)
0
100
200
300
400
1000
1200
1400
Time (hr)
NPP 1-Fines
NPP 1-16
SPP 2-18
SPP 2-Fines
SPP 2-16
NPP 1-8
NPP 1-20

Figure 10.

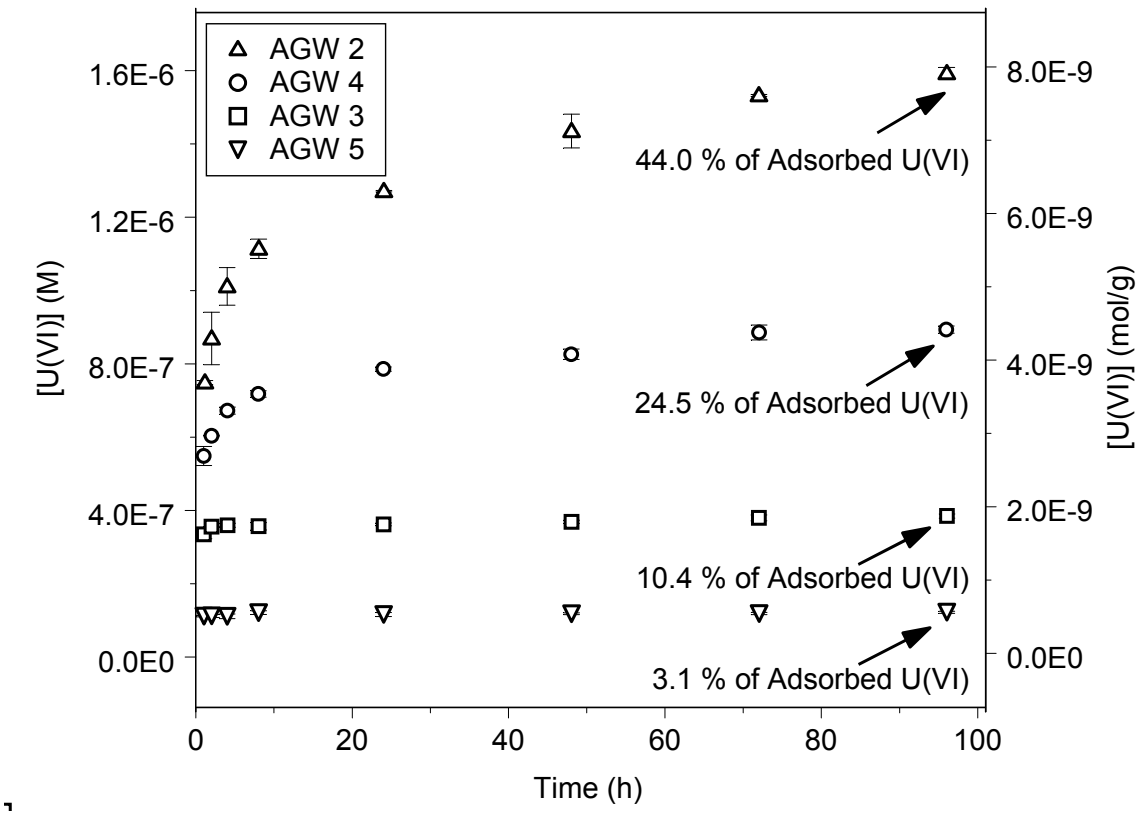
AGW 2
AGW 4
AGW 3
AGW 5
44.0 % of Adsorbed U(VI)
24.5 % of Adsorbed U(VI)
10.4 % of Adsorbed U(VI)
3.1 % of Adsorbed U(VI)
[U(VI)] (M)
[U(VI)] (mol/g)
Time (h)
1.6E-6
1.2E-6
8.0E-7
4.0E-7
0.0E0
8.0E-9
6.0E-9
4.0E-9
2.0E-9
0.0E0
0
20
40
60
80
100

Figure 11.

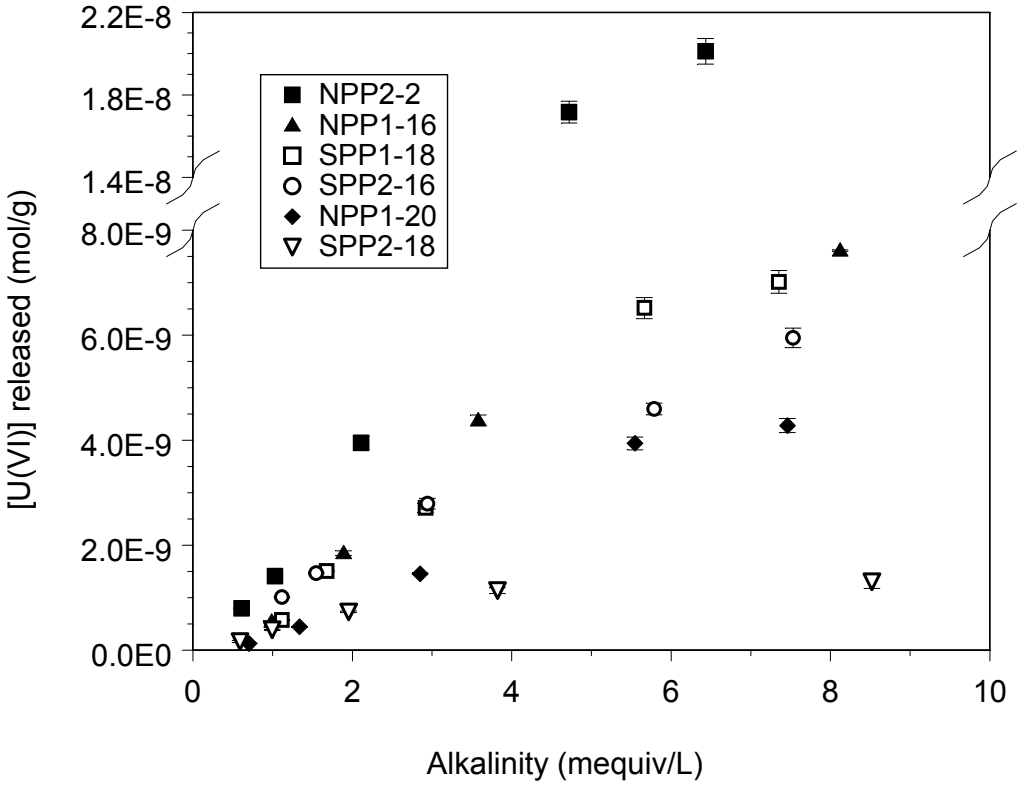
2.2E-8
1.8E-8
1.4E-8
8.0E-9
6.0E-9
4.0E-9
2.0E-9
0.0E0
[U(VI)] released (mol/g)
0
2
4
6
8
10
Alkalinity (mequiv/L)
NPP2-2
NPP1-16
SPP1-18
SPP2-16
NPP1-20
SPP2-18

Figure 12.

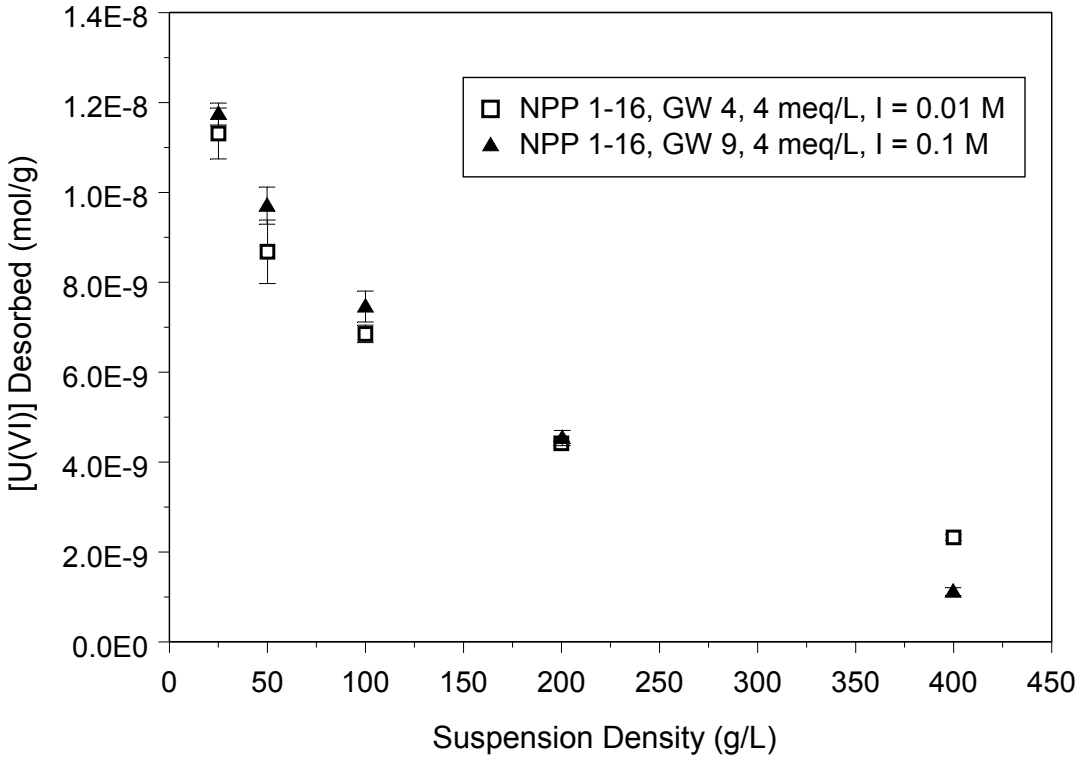
1.4E-8
1.2E-8
1.0E-8
8.0E-9
6.0E-9
4.0E-9
2.0E-9
0.0E0
[U(VI)] Desorbed (mol/g)
0
50
100
150
200
250
300
350
400
450
Suspension Density (g/L)
NPP 1-16, GW 4, 4 meq/L, I = 0.01 M
NPP 1-16, GW 9, 4 meq/L, I = 0.1 M

Figure 13a.

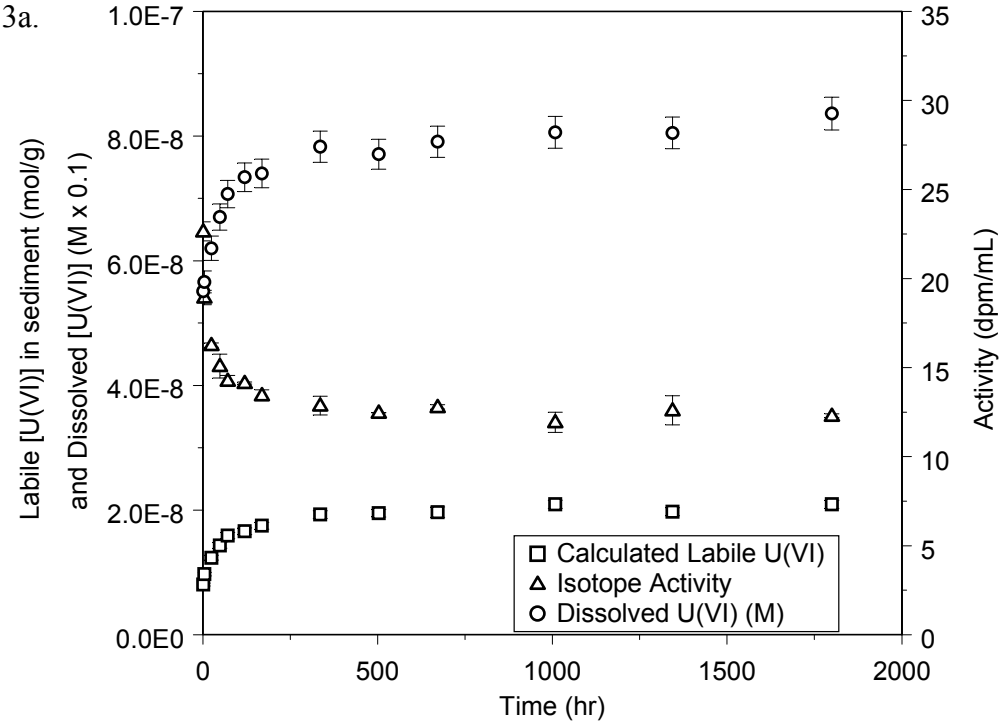

Figure 13b.

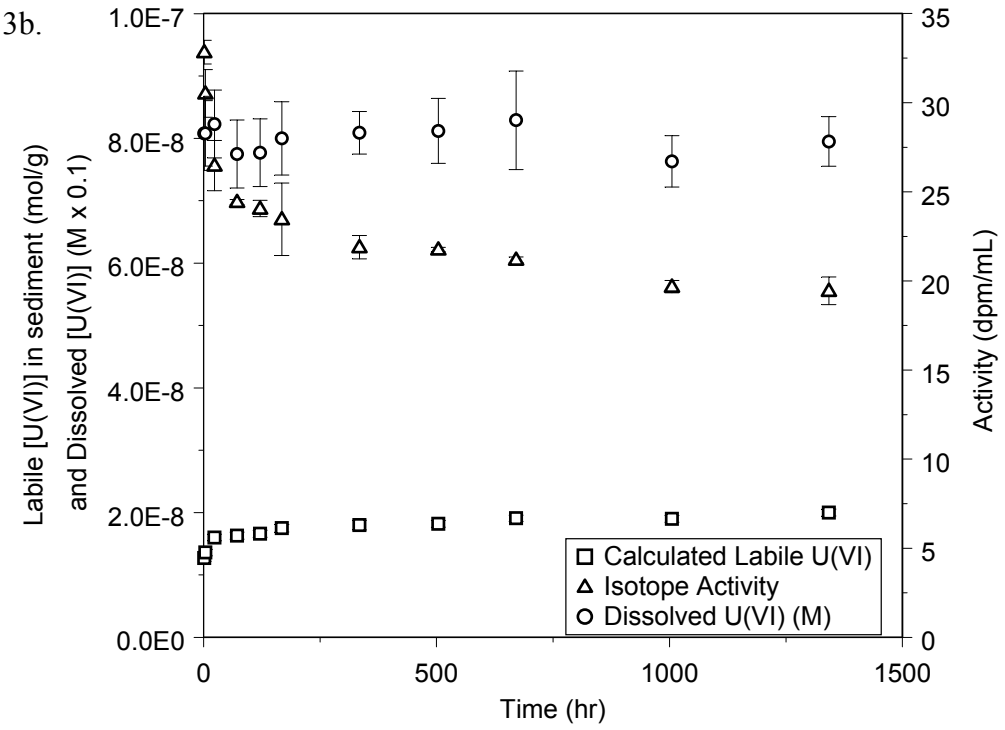

Figure 14a.

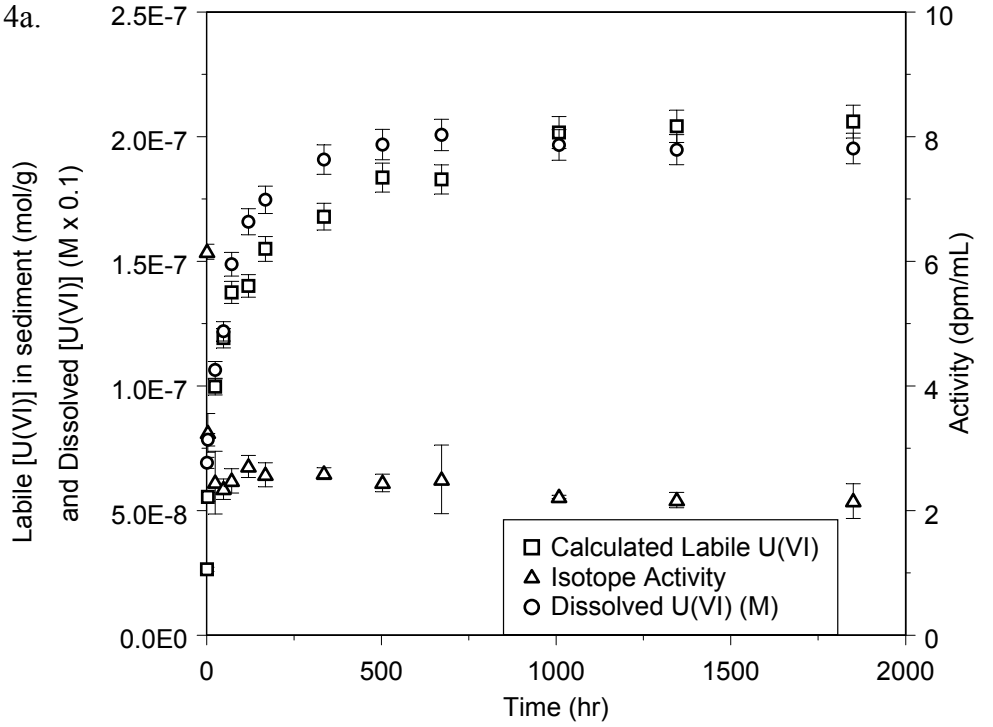

Figure 14b.

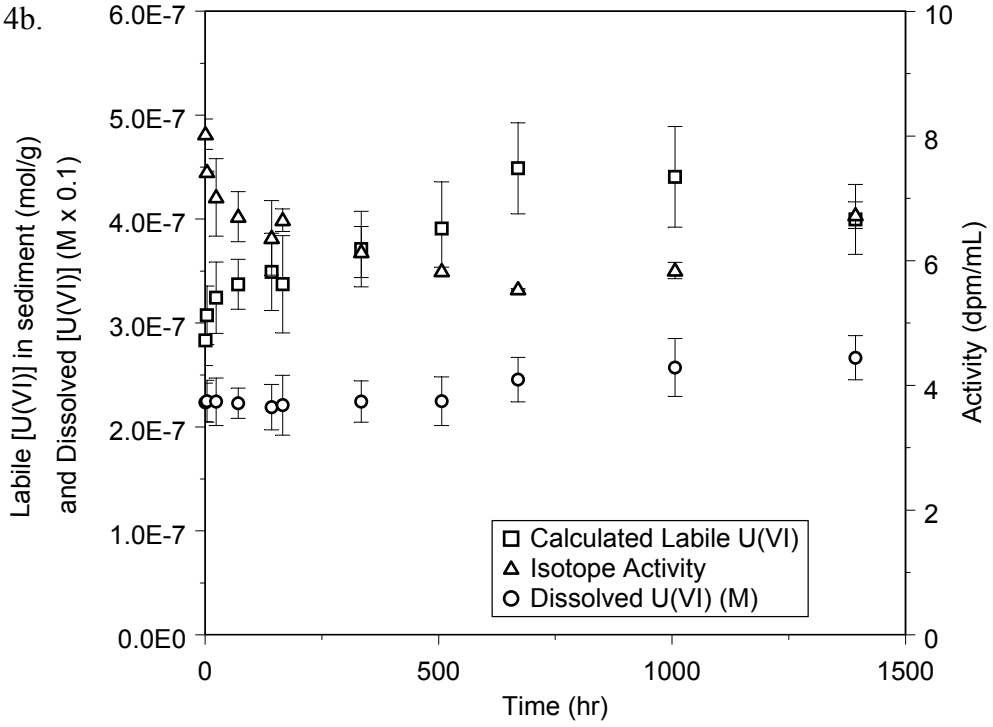

Figure 15.

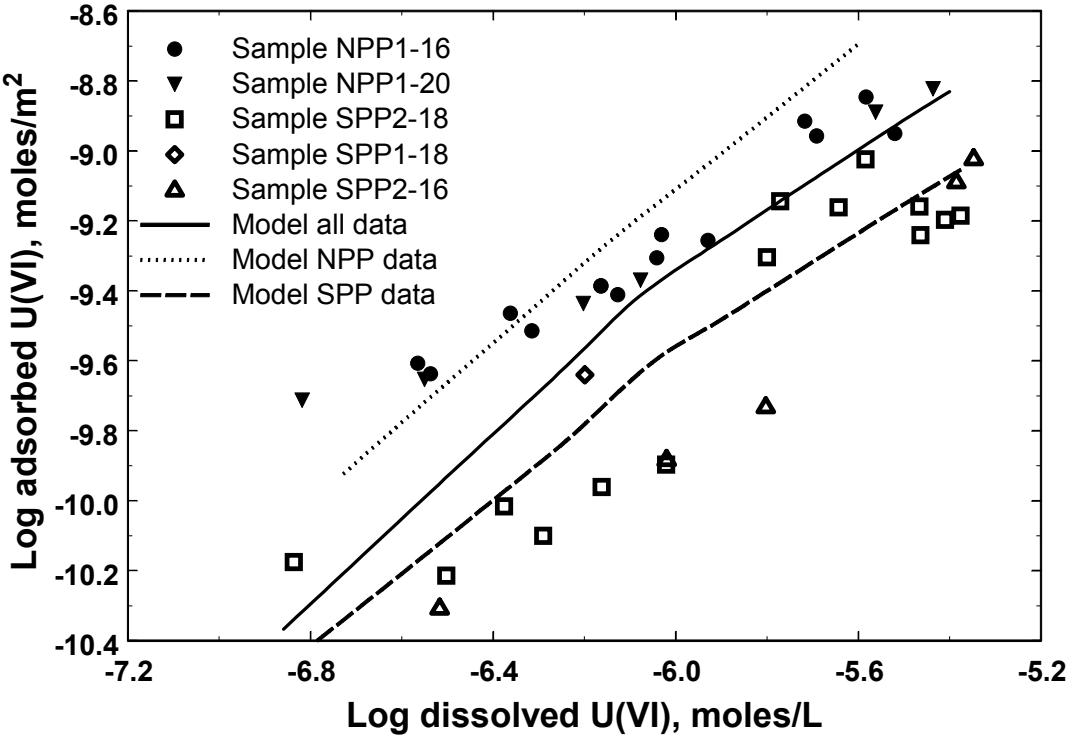
Sample NPP1-16
Sample NPP1-20
Sample SPP2-18
Sample SPP1-18
Sample SPP2-16
Model all data
Model NPP data
Model SPP data
Log adsorbed U(VI), moles/m2
Log dissolved U(VI), moles/L
-8.6
-8.8
-9.0
-9.2
-9.4
-9.6
-9.8
-10.0
-10.2
-10.4
-7.2
-6.8
-6.4
-6.0
-5.6
-5.2

Figure 16.

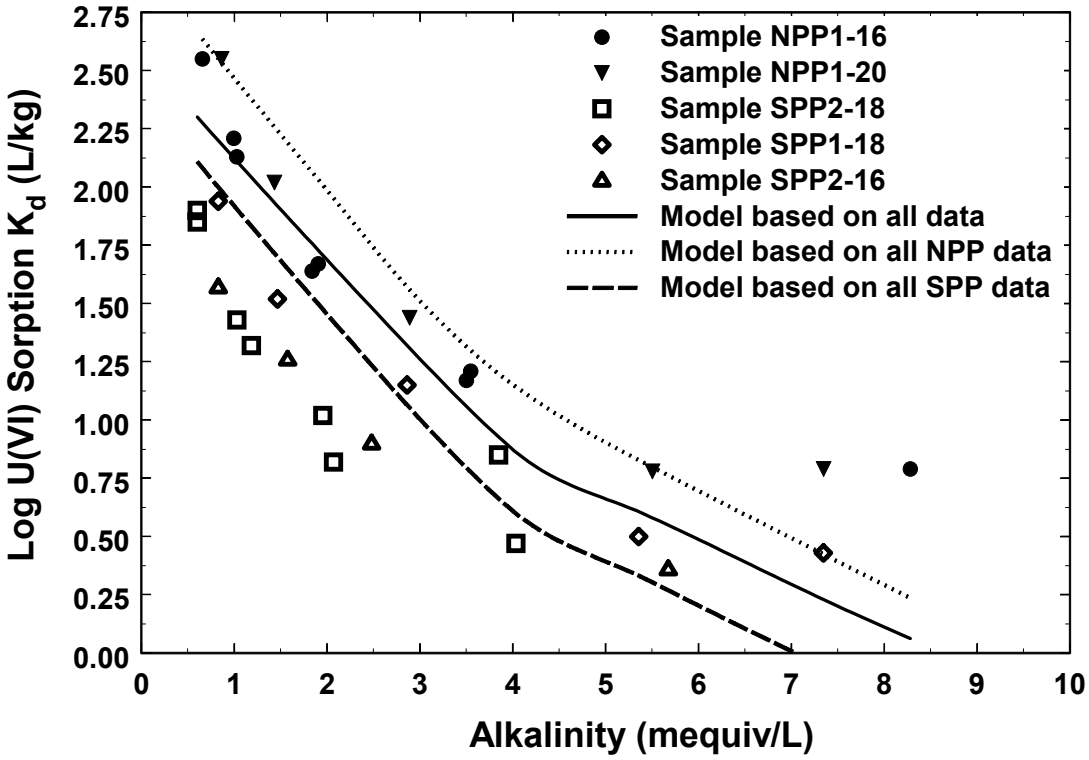
Log U(VI) Sorption K_d (L/kg)
Alkalinity (mequiv/L)
Sample NPP1-16
Sample NPP1-20
Sample SPP2-18
Sample SPP1-18
Sample SPP2-16
Model based on all data
Model based on all NPP data
Model based on all SPP data
0.00
0.25
0.50
0.75
1.00
1.25
1.50
1.75
2.00
2.25
2.50
2.75
0
1
2
3
4
5
6
7
8
9
10